RESONANCE LINE FORMATION IN EXPANDING DECELERATING ATMOSPHERES

Dissertation for the Degree of Ph. D.
MICHIGAN STATE UNIVERSITY
FELIX MARTI
1977



This is to certify that the

thesis entitled

RESONANCE LINE FORMATION

IN EXPANDING DECELERATING ATMOSPHERES

presented by

Felix Marti

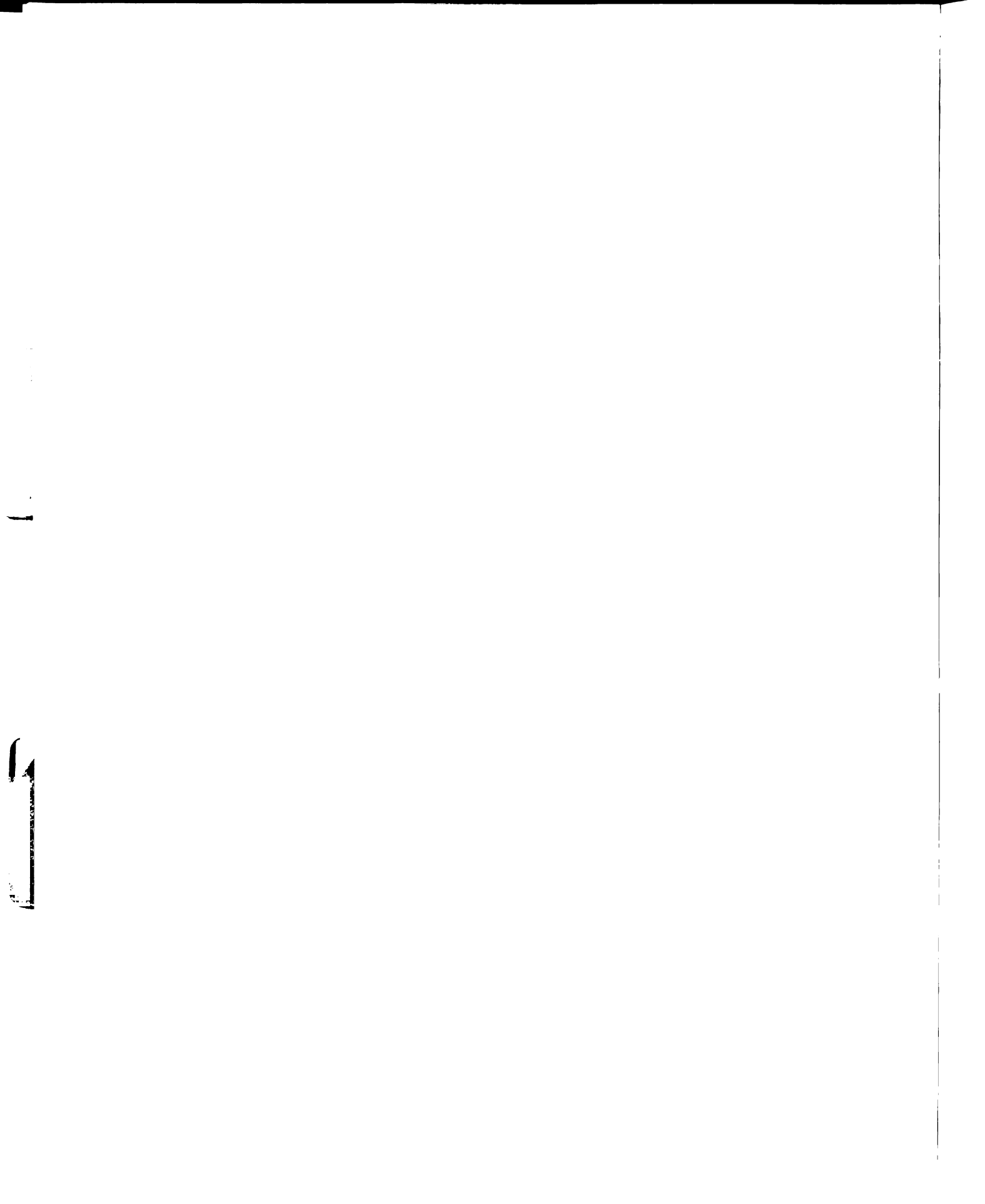
has been accepted towards fulfillment of the requirements for

PhD degree in Physics

Major professor

Date ____5/6/77

O-7639



ABSTRACT

RESONANCE LINE FORMATION IN EXPANDING DECELERATING ATMOSPHERES

Βv

Felix Marti

We study the formation of resonance lines in a stellar atmosphere that is expanding but decelerating, or infalling and accelerating as it falls in. Spherical geometry is taken into account, and we assume the supersonic approximation with complete redistribution over the line profile in the fluid frame. Various layers in the atmosphere become radiatively coupled or interconnected, because of Doppler shifts and effects of the projection of the velocity on the ray direction. The line profiles show sharper and sharper peaks as the outer cutoff radius is increased, or the velocity law is steepened. It is possible to obtain profiles with as sharp a drop-off at the blue of the peak as is seen in the QSO PHL 5200. Some profiles with emission in the envelope are qualitatively like those found by Walker for young stars with infalling matter. The profiles disagree with recent observations by Hutchings for one sample of P Cygni stars, showing that the decelerating model does not apply to this sample. The approximate method of Kuan and

Kuhi, which neglects the coupling between layers, turns out to be generally acceptable for finding the source function, as they proposed, but would lead to qualitatively wrong results if applied to find the radiative acceleration. We find that their suggested criterion for validity of the approximation is questionable, and we give better criteria.

We construct "pictures" of what the star would look like in two dimensions, in anticipation of interferometry or occultation work, but find that the appearance is annoyingly similar in different wavelength bands.

RESONANCE LINE FORMATION IN EXPANDING DECELERATING ATMOSPHERES

Ву

Felix Marti

A DISSERTATION

Submitted to

Michigan State University
in partial fulfillment of the requirements
for the degree of

DOCTOR OF PHILOSOPHY

Department of Physics

ACKNOWLEDGEMENTS

I am most grateful to Professor Peter D. Noerdlinger for suggesting the topic of this dissertation, and for his ideas, patient guidance, and encouragement throughout the whole work, making it an enjoyable learning process.

I would also like to express my gratitude to Dr. Morton M. Gordon for his support and friendship during my graduate study years at Michigan State.

I thank the College of Natural Science for financial support during the last period of this work.

I am indebted to Drs. David Hummer and George B. Rybicki for communicating results of their unpublished work that enabled me to detect a programming error.

I thank The University of Chicago Press for granting us authorization to reproduce Figures 2 through 6, 9 through 19, and 21 through 24.

And finally many thanks to all the people who contributed in many ways to make this possible, and made my stay in East Lansing a very enjoyable experience, and especially to my wife Elida and my family.

TABLE OF CONTENTS

LIST OF F	IGURES	iν
CHAPTER		
I.	INTRODUCTION	1
	Previous Work	1
II.	SOLUTION OF THE EQUATION OF TRANSFER	9
	Mean Intensity and Source Function	9 1 4 2 9 3 4 3 7
III.	RESULTS OF THE COMPUTATIONS AND COMPARISON	
	WITH OBSERVATIONS	39
	Source Function	39 40 50 60 82
IV.	CONCLUSIONS AND FUTURE WORK	93
		9 3 9 5
APPENDIX		
Α.		97
В.		0 4
С.		0 7
REFERENCES	S 1	1 N

LIST OF FIGURES

FIGURE		Page
1.	a, b, and c, are the surfaces able to interact with the atoms at A, B, and C respectively. The velocity law is $v = v_o(r_c/r)$. 13
2.	Constant velocity surfaces for an accelerating atmosphere. The velocity law is $v(r) = v_{\infty}(1-r_{c}/r)^{\frac{1}{2}}$. The numbers indicate the ratio v_{z}/v_{∞} for each curve	. 18
3.	Constant velocity surfaces for a decelerating atmosphere. The velocity law is $v(r) = v_0(r_c/r)$. The numbers indicate v_z/v_0 . A line parallel to the observing direction intersects these surfaces once, twice, or	
4.	The straight line defined by the observer and the center of the star is the z axis, with its origin at the center of the star and the positive direction away from the observer. The intersection of the photospheric radius r _c and line with impact parameter p has abscissa z _c . For each sphere of radius r, there are two surfaces of constant velocity v _z that have tangents at the intersection points parallel to the z axis; those intersections have abscissas z' _d and z'' _d . z _e is the abscissa of the intersection of the line with impact parameter r _c and the sphere of radius r on the negative side of	. 21
	the z axis	. 23

Figure		Pa	ıge
11.	Comparison between the exact solution (solid curve) and the disconnected approximation of the force for a star with RR = 10, $r_c = 10 R_o$, $\tau_{04} = 100$, $B = 5 I_c$, $\ell = 0.5$, and $\ell = 100$, and $\ell = 100$.	•	57
12.	Comparison between the exact solution (solid curve) and the disconnected approximation of the force for a star with RR = 10, $r_c = 10 R_o$, $\tau_o = 1000$, $\epsilon = 0.001$, $E = 5 I_c$, $\ell = 0.5$, and $E = 10^{-3}$	•	59
13.	Comparison of the line profile in the exact solution (solid curve) and the disconnected approximation. The τ given is τ_0 . The ab-		
14.	scissa is $(v-v_0)/\Delta v_m$ where $\Delta v_m = (v_0/c)v_0$. Comparison of two line profiles for atmospheres with $\tau_0 = 50$, $\epsilon = 0.001$, $B(r) = I_c(r_c/r)^{\frac{1}{2}}$, and $\ell = 0.5$. Curve a corresponds to an atmosphere with RR = 10, (equivalent width (EW) = -0.410); curve bhas RR = 3, (EW = -0.0739). Note that the case $\ell = 1$ is expected to be more sensitive		
15.	to the value of RR (see text)		
16.	Profiles for three atmospheres with RR = 10, ϵ = 0, ℓ = 0.5, and τ_0 as indicated. Curve <u>a</u> : EW = 0.0050, curve <u>b</u> : EW = 0.0086, curve <u>c</u> : EW = 0.0028		
17.			

Figure		Pa	ıge
18.	Upper: Copernicus scans of individual stars from 1165 to 1255 Å, smoothed over 1 Å. Center: unsmoothed mean spectrum of all stars in upper section, with continuum drawn in. Lower: mean of 11 scans of C III λ 1175 for P cyg and ξ^1 Sco		76
19.	The dots represent the observed profiles of the resonance lines (normalized to v_{∞} = 2660 km/s) of Zeta Puppis	•	79
20.	•	•	81
21.	p I_{tot} and p I_r versus p/r_m for a star with RR = 3, τ_o = 50, ε = 0.001, B = I_c , and ℓ = 0.5	•	84
22.	p I_{tot} and p I_r for a star with RR = 10, τ_0 = 100, ϵ = 0.001, B = 5 I_c , and ℓ = 0.5.	•	86
23.	p I tot and p I for a star with RR = 10, τ_0 = 1000, ϵ = 0.001, B = 5 I c, and ℓ = 0.5.	•	88
24.	p I _{tot} and p I _r for a star with RR = 10, $\tau_0 = 1000$, $\epsilon = 0.001$, B(r) = 5 I _c (r _c /r), and $\ell = 0.5$. Note that all the parameters but B coincide with the parameters in		0.0
	Figure 16	_	90

CHAPTER I

INTRODUCTION

Previous Work

There has been a permanent interest among astronomers on the problem of spectral line formation in expanding or contracting media. We have numerous examples of objects that are apparently expelling material in a steady way or in bursts: Wolf-Rayet, P Cygni, Be, Of stars, Novae, Seyfert galaxies, and possibly some QSOs.

The presence of a P Cygni type profile (emission peaked at the central frequency of the line and a violet displaced absorption feature) in the spectrum of a star is interpreted as an indication of the existence of material around the star that is moving away from it. Due to the Doppler shift this material will see radiation emitted at the central frequency of the line in the observer's (laboratory) frame displaced toward the red and will absorb more of the radiation in the violet wing of the central peak, producing the absorption dip observed in the high frequency side of the line.

Milne (1926) was the first one to point out the possibility of ejection of particles by hot stars due to unbalanced radiation pressure. He assumed that initially the

atom is in equilibrium with the radiation in the deep part of the absorption line, then an accidental motion outward makes the atom absorb in the violet wing where the intensity is larger, thus accelerating it further.

After Beals (1929,1930,1934) established the model of an expanding extended atmosphere to explain the spectra of Wolf-Rayet stars, Gerasimovic (1933), Chandrasekhar (1934, 1945), and McCrea and Mitra (1936), made the first attempts to develop a theory that could explain quantitatively the observed profiles. We must notice that both Gerasimovic and Chandrasekhar considered the case of a decelerating atmosphere as well as the accelerating one. Gerasimovic found a velocity law of the form $r^{-\frac{1}{4}}$ for the expansion of the hydrogen shell in Nova Aquilae four days after the maximum. Both authors assumed complete transparency and that the emission per unit volume was known, neglecting then the transfer problem.

The next step toward the solution came when Sobolev (1958,1960) developed a simple theory applicable in cases where the macroscopic velocity of the material in the atmosphere is much larger than the mean thermal speed. Rublev (1961,1963) applied this formulation to the interpretation of the spectra of Wolf-Rayet stars and also studied the case of decelerating flows (Rublev 1964). He computed the line profiles assuming that the emission and absorption components of the bright lines are formed in the same spherical layer of the envelope, and that the corresponding

coefficients vanished everywhere else.

Kuhi (1964) applied Chandrasekhar's method to T-Tauri stars considering that after leaving the stellar surface, the atoms were subjected only to the force of gravity, decelerating the flow after the initial thrust. The coefficient of emission was assumed known.

Castor (1970) gave the first solution that allowed one to determine the emission coefficient in a self-consistent way, in the case of an accelerating atmosphere. Castor and Van Blerkom (1970) applied it to the He II lines in Wolf-Rayet stars, and Castor and Nussbaumer (1972) to C III in the same type of stars. Oegerle and Van Blerkom (1976a,b) have studied the neutral Helium lines in Wolf-Rayet and P Cygni envelopes using the same formalism.

Our Approach

As we see, most of the recent work done using Sobolev and Castor's escape probability method is restricted to accelerating flows, probably because these flows are by far the most common and the most relevant to understanding stellar winds and mass loss from stars. Nevertheless, there remains considerable interest in studying other possibilities, such as outflows that decelerate, inflows that speed up under the influence of gravity as they near the star or central object, and more complicated velocity fields. In the flows just mentioned, and more complex ones, such as rotating flows or those with shocks, there will generally be fairly distant parts of the flow that are in touch with each

other rather closely through the radiation field, since the relevant radiation travels freely through the intervening material. The reasons for this are shown in some detail in Chapter II, but rest simply on the fact that Doppler shifts can cause distant parts of the gas to contribute opacity at the same laboratory frame frequency, while in simpler monotonically accelerating flows, the radiation at one laboratory frequency can interact with the gas only in one small connected region. The coupling of distant regions has been emphasized by Hummer (1976).

There are at least three reasons for our interest in such flows: the decelerating flow has been claimed by Kuan and Kuhi (1975) to explain the hydrogen profiles in P Cygni stars better than the standard accelerating flows; there is evidence for infall of matter in such objects as θ^1 Ori C (Conti 1972) and several stars described by Walker (1968, 1972); and finally, systems such as we study here are of intermediate complexity between the accelerating outflow and the cases with rotation or shocks; hence we may gain experience useful in the harder cases.

Kuan and Kuhi (1975) coupled a multi-level populations calculation with the escape probability method of Sobolev and Castor to find the source function S(r). In common with Kuan and Kuhi, we adopt the supersonic approximation. In this approximation, assuming complete redistribution over the line profile, one finds (Castor 1970) that the source function is frequency independent, and can be related in a

simple way to the incident stellar continuum I_c and the quantity \overline{J} defined as the mean intensity J_x , integrated over the fluid-frame line profile $\phi(x)$

$$\overline{J} = \int_0^\infty J_x \phi(x) dx, \qquad J_x = \frac{1}{4\pi} \int I_x d\omega , \qquad (I-1)$$

where x is the frequency in the fluid frame. (In multilevel problems, \overline{J} and S will have subscripts, usually suppressed here.) An analysis of populations, or a simplifying assumption such as that of the two-level atom (adopted here), leads to relationships among the various \overline{J}_{ij} , S_{ij} , and the continua, but the transfer equation itself must be applied to close the system of equations, because the local excitation depends on transfer to and from the region under study. For an accelerating expanding atmosphere, Castor (1970) showed that this closure is obtained <u>locally</u> (zone by zone, i.e. at each radius r in the atmosphere separately) by the equation

$$\overline{J} = (1 - \beta)S + \beta_C I_C , \qquad (I-2)$$

where β is the escape probability and β_{C} the escape probability in the cone of solid angle occupied by the stellar photosphere (see Castor (1970) and Chapter II below).

Equation (I-2) shows that the integrated mean intensity at a point is a weighted combination of the local source function and a contribution from the photospheric continuum; i.e. it contains light emitted locally and incident light. Clearly, when Doppler shifts allow light from one part of the atmosphere to interact again in another, additional

-	-
	•
	1
	Ì
	:

terms coupling the layers must be present. In Chapter II, we show explicitly how a coupled set of linear equations, relating S(r) in the various layers of different r, replaced (I-2) for a decelerated atmosphere. In a later paper, Kuan (1975) alluded to this interconnection, but stated that it was a "justifiable approximation" to ignore it "if the radiation field in the envelope is weak in comparison with the photospheric intensity, which is usually the case". We point out here that this statement is valid insofar as one has radiation from one part of the envelope adding to the excitation in other parts; however, one also has parts of the extended atmosphere masking other parts from the central continuum.

Our primary thrust is to study the influence of the interlayer radiative coupling, and so verify in what cases the approximation of Kuan and Kuhi (hereinafter called the "disconnected approximation") applies. Furthermore, we evaluate the radiation force on the material, and comment on the applicability of decelerating atmospheres to real stars. In order to test the effect of the "disconnected approximation" we have arranged our analysis to turn the interlayer radiative coupling on and off at will.

One naturally asks how valid the assumption of the two level atom is for real stars. We note that in the cases considered by Kuan and Kuhi as strong candidates for decelerating flow, the Balmer lines have large emission, with small absorption features. Under their assumptions such net

emission must come from the expanding envelope. No matter what the excitation process, then for Balmer lines the radiation field due to the envelope is a fortiori strong compared with the photospheric continuum; furthermore, if the excitation is partly Lyman flouresence, as is likely, the interlayer coupling for Lyman radiation is also strong, and could importantly affect the Balmer profiles.

The specific cases we study are the velocity laws

$$v(r) = \pm v_0 (r_c/r)^{\ell}, \qquad (I-3)$$

where r_c is the radius of the opaque core (photosphere), v_o the largest velocity in the atmosphere, and the two choices $\ell=1$ and $\ell=\frac{1}{2}$ were considered. The case $\ell=\frac{1}{2}$ and $\ell=\frac{1}{2}$ and

In all cases, mass conservation

$$N_i r^2 v(r) = const.,$$
 (I-4)

was assumed, where N_i is the number density. (This fails to allow for changes in the state of ionization, since N_i actually will represent a specific ion.)

According to equations (I-3) and (I-4) the material does not thin out as fast with increasing radius as in an accelerating flow. For computational reasons, a cutoff is

introduced at some radius r_m . This cutoff, which seems artificial, has considerable influence on the resonance line profiles, in contrast to Kuan and Kuhi's case of subordinate lines. Typical times to traverse an atmosphere of radius 10^{13} cm at a thousand km/s are of the order of a day. Therefore, the true radius is much larger than what is used, and we must regard the cutoff as due to a change in state of ionization. If the velocities accelerated again past r_m this could help thin out the material and so reduce the influence of the cutoff.

In summary, we will be studying the formation of resonance lines in expanding or contracting atmospheres with velocity fields given by equation (I-3). We assume the photospheric core where the continuum (with no limb darkening) is formed to have radius \mathbf{r}_{C} , and the expanding envelope extends from \mathbf{r}_{C} up to \mathbf{r}_{m} . We will use the two level atom approximation of the source function. The absorption profile is taken to be extremely sharp (the macroscopic velocities are much larger than the thermal velocities). We tried to express our results in such a way that allows us to use them with different sets of parameters that satisfy certain scaling laws. The atomic data we use correspond to the C IV $\lambda 1550$ resonance line.

CHAPTER II

SOLUTION OF THE EQUATION OF TRANSFER

Fluid Frame Picture

In this work we will assume that the thermal width of the line is negligible and take it as practically zero.

This assumption allows us to study the formidable problem of transfer of radiation in a simple formulation similar to Sobolev and Castor's.

Several papers have been published on the problem of an accelerating atmosphere using a more accurate formulation than ours, without making the assumption of zero thermal width. In such a case it is convenient to solve the equation of transfer in the frame co-moving with the fluid as was indicated already by McCrea and Mitra (1936). Consider for example (Hummer 1976) the integrated mean intensity

$$\overline{J} = \frac{1}{4\pi} \int_{-\infty}^{+\infty} dx \int_{-1}^{+1} d\omega \, \phi(x - \overrightarrow{u} \cdot \widehat{n}) I_{x}(\widehat{n}), \qquad (II-1)$$

where x is a dimensionless frequency referred to the line center (see formula A-17), u is the fluid velocity in units of the thermal velocity (formula A-20), and $\vec{u} \cdot \hat{n} = \mu |u|$. Even if $\phi(y)$ is different from zero in a small region about y = 0, in the observer's frame we have to consider a large region in the (x,μ) plane that will contribute to the integral for large u. The size of the mesh of points required

to solve the equation of transfer is therefore much larger in the observer's frame than in the co-moving frame.

The differential equation in the co-moving frame (see equation A-30) is significantly more complicated than the corresponding one in the observer's frame (in the stationary frame, the frequency derivative, $\partial I_{\chi'}/\partial x'$, is absent). An additional difficulty appears when we try to find the intensity emitted by the envelope at a <u>fixed observer's frequency</u>, because the solution was obtained in principle with the comoving frequency as a variable.

Noerdlinger and Rybicki (1974) gave the first stable scheme for the numerical solution in the co-moving frame for the case of a plane parallel atmosphere, that was developed later to the spherically symmetric case by Mihalas, Kunasz, and Hummer (1975,1976a,1976b).

Consider an observer carried outward in a spherically symmetric velocity field v(r). He observes his neighbors located a distance ds away in the radial direction to have velocity relative to him $d\xi = (dv/dr)ds$, while neighbors at the same distance from the center are departing at a rate $d\eta = (v/r)ds$. If dv/dr > 0, then $d\xi$ and $d\eta$ have the same sign, and the fluid expands in all directions. If not, the fluid is compressed in one dimension and it expands in the other; for some intermediate directions neighboring particles maintain constant separation to first order. These two possibilities lead to vast differences in radiative transfer. In the former case, a light quantum repeatedly absorbed and

emitted in a region will constantly encounter fluid moving away from it; hence it must eventually escape in the red wing of the line in the fluid frame (if it does not escape due to density gradients, or become buried back in the central source). (If $d\xi$ and $d\eta$ are both negative, replace "away" by "toward" and "red" by "blue" in the foregoing.)

Figure 1 shows the loci of points that have zero velocity of approach with respect to the moving points A, B, C. The velocity law is given by equation (I-3) with $\ell=1$. Consider a set of observers that are moving with the fluid, like the ones sitting on points A, B, and C. If they can detect light only through a narrow band filter centered at the line frequency ν_0 , they will see light from that transition coming only from points in the atmosphere that have zero relative velocity in the direction that joins them with the emitting points. Figure 1 shows the surfaces a, b, c, of zero relative velocity in the connecting direction with respect to observers A, B, and C respectively. The velocity law is given by equation (I-3) with $\ell=1$.

In the case of an accelerated atmosphere the picture is completely different. The observers will see light coming only from a small region around them, they will not be "connected" to the rest of the atmosphere, and the excitation at each point can be found locally (it will also depend on the continuum intensity I_c).

Our next step will be to find an integral equation for the source function, but before, assuming S(r) as known we

Figure 1. a, b, and c, are the surfaces able to interact with the atoms at A, B, and C respectively. The velocity law is $v = v_0(r_c/r)$.

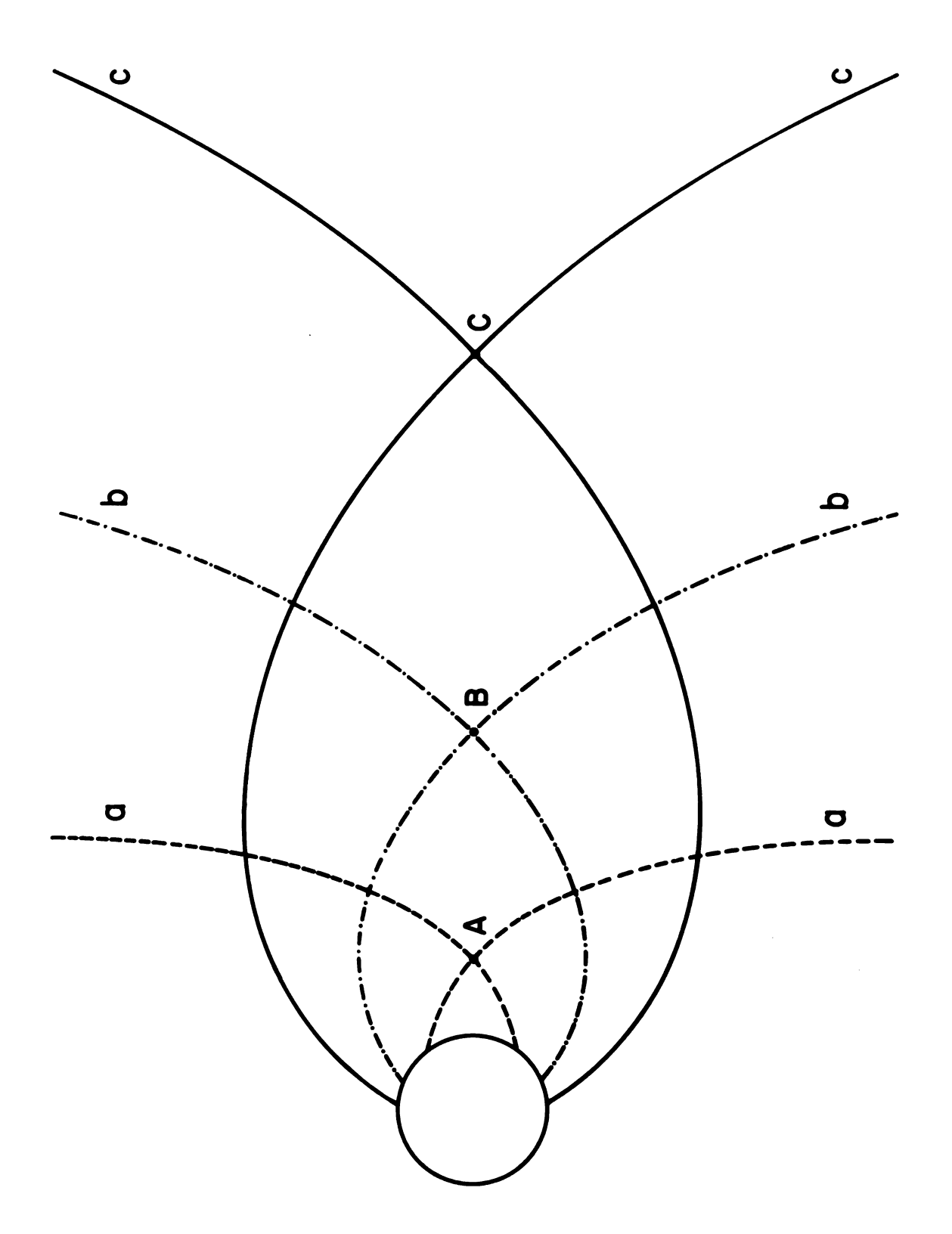


Figure 1

find an expression for the specific intensity I, the so called "formal integral".

The Formal Integral

Following Castor's (1970) notation, we use a cylindrical coordinate system (p, θ, z) where the z axis is the line joining the center of symmetry of the atmosphere and the observer, with the positive direction away from the observer and the origin at the center of the star. Note that p is the impact parameter. We define

$$r^2 = p^2 + z^2$$
. (II-2)

That is, r is the radial distance measured from the center of the star. If the absorption and emission of radiation within the line are uncorrelated both in angle and frequency (complete redistribution) in the fluid frame, the source function will be independent of frequency. The equation of transfer takes the form (Castor 1970)

$$\frac{\partial I(v,p,z)}{\partial z} = k(v,p,z)[I(v,p,z) - S(r)], \qquad (II-3)$$

where I is the specific intensity directed toward the observer as seen at the point with impact parameter p and abscissa z. This equation is a simple modification of our (A-7).

The photosphere lies at $r=r_{c}$ and is supposed to radiate a continuous spectrum I_{c} with no limb darkening. Then the formal solution of the transfer equation is

$$-e^{-\tau(\nu,p,z)}I(\nu,p,z)\Big|_{\tau(z)}^{\tau(\infty)} =$$

$$\int_{\tau(z)}^{\tau(\infty)} S[(p^{2}+z^{2})^{\frac{1}{2}}]e^{-\tau(\nu,p,z^{2})}d\tau(\nu,p,z^{2}), \qquad (II-4)$$

where the integral is done at constant ν and p, and $d_{\tau}(\nu, p, z) = k(\nu, p, z) dz$.

If $p > r_c$, or z > 0 the integration path will not intersect the core and we get

$$I(v,p,z) =$$

$$\int_{z}^{\infty} S[(p^{2}+z'^{2})^{\frac{1}{2}}] \exp[\tau(v,p,z)-\tau(v,p,z')]d\tau. \qquad (II-5)$$
 But if p < r_c and z < 0

$$I(v,p,z) =$$

$$\int_{z}^{z_{c}} S[(p^{2}+z'^{2})^{\frac{1}{2}}] exp[\tau(v,p,z)-\tau(v,p,z')] d\tau(v,p,z')$$

+
$$I_c \exp[\tau(v,p,z)-\tau(v,p,z_c)],$$
 (II-6)

where
$$z_c = -(r_c^2 - p^2)^{\frac{1}{2}}$$
. (II-7)

The optical depth along a line of constant impact parameter p, from the location z to the observer is given by

$$\tau(v,p,z) = \int_{-\infty}^{z} k(v,p,z') dz', \qquad (II-8)$$

where the absorption coefficient is

$$k(v,p,z) = k_{\ell}(r) \phi[v-v_0+v_0\beta(r) z r^{-1}].$$
 (II-9)

Note that the zr^{-1} term comes from the projection of the

radial velocity in the observer's direction. Here, $\beta(r) = v(r)/c, \text{ and } \phi \text{ is the line profile in the fluid frame,}$ normalized as

$$\int_{-\infty}^{\infty} \phi(x) \, dx = 1 \quad ; \quad x = v - v_0 + v_0 \, \beta \, z \, r^{-1}, \quad (II-10)$$

and k_{ℓ} , the line absorption coefficient between levels 1 (lower) and 2 (upper), depends on r only:

$$k_{\ell} = (N_1 B_{12} - N_2 B_{21}) \frac{h_{00}}{4\pi} = g_2 B_{21} (\frac{N_1}{g_1} - \frac{N_2}{g_2}) \frac{h_{00}}{4\pi},$$
 (II-11)

where the B's are the Einstein's coefficients and the g's the statistical weights of the respective levels. Introducing the absorption oscillator strength f_{12} (Mihalas 1970)

$$g_2 B_{21} = g_1 B_{12} = g_1 f_{12} \frac{4\pi^2 e^2}{h\nu_0 mc}$$
, (II-12)

and finally

$$k_{\ell} = \frac{\pi e^2}{mc} (gf) (\frac{N_1}{g_1} - \frac{N_2}{g_2}).$$
 (II-13)

We shall assume that the line profile is extremely sharply peaked at x=0 (frequency = v_0 in the rest frame of the gas), so that τ is essentially a combination of step functions. The number of "steps" to the step function is the number of intersections of the line of sight with the surface of constant z velocity.

Chandrasekhar (1934) seems to have been the first one to construct surfaces of constant line of sight velocities as seen by an external observer looking at a monotonically accelerating atmosphere, Figure 2. Note that a line parallel to the line of sight intersects such a surface just at

Figure 2. Constant velocity surfaces for an accelerating atmosphere. The velocity law is $v(r) = v_{\infty}(1-r_{c}/r)^{\frac{1}{2}}$. The numbers indicate the ratio v_{z}/v_{∞} for each curve.

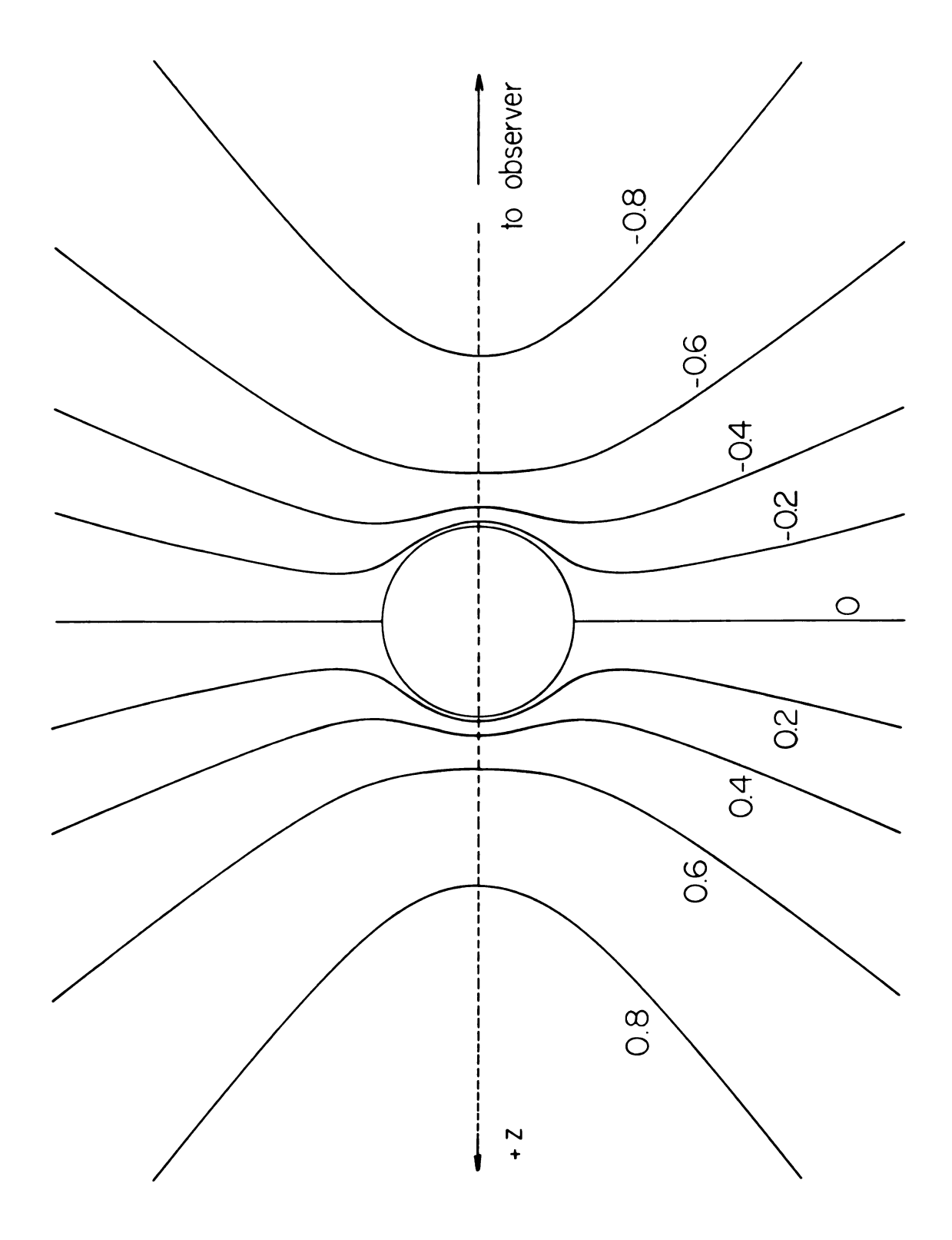


Figure 2

3

n t

t; or

ab th

ca ti

Not

:,

one point. If the flow is a decelerating expansion, the constant velocity surfaces appear as in Figures 3 and 4. We see that in this case there can be 0, 1, or 2 intersections.

In the region close to each intersection, the contribution to the integral in equation (II-8) is

$$\tau_{i}(p,v) = \int_{z_{i}-\delta}^{z_{i}+\delta} k(v,p,z')dz' =$$

$$k_{\ell}[(p^{2}+z_{i}^{2})^{\frac{1}{2}}] \int_{z_{i}-\delta}^{z_{i}+\delta} \phi(v-v_{o}+v_{o}\beta(r)zr^{-1})dz =$$

$$\frac{k_{\ell}[(p^{2}+z_{i}^{2})^{\frac{1}{2}}]}{\left|(\frac{\partial x}{\partial z})p,\nu\right|_{z=z_{i}}} \int \phi(x) dx = \frac{k_{\ell}[(p^{2}+z_{i}^{2})^{\frac{1}{2}}]}{\left|(\frac{\partial x}{\partial z})p,\nu\right|_{z=z_{i}}} i=1,2 , (II-14)$$

where δ is selected to pick up all the contribution to the opacity from each intersection. The derivative in the denominator is the Jacobian of the change of variables from z to x.

Figure 5 shows the definition of some unit step functions γ_i , that we find useful in describing the variation of optical depth with z. When some of the intersections are absent, the corresponding τ should not be included, and in the following formulae this should be done by setting the corresponding τ equal to zero. When there are two intersections, τ has the form

$$\tau(v,p,z) = \tau_1(p,v) \gamma_1(z) + \tau_2(p,v) \gamma_2(z).$$
 (II-15)

Note that $\gamma(z)$ stands for $\gamma[x(z)]$ where x is the argument of ϕ , that is the frequency in the fluid frame. The behavior

Figure 3. Constant velocity surfaces for a decelerating atmosphere. The velocity law is $v(r) = v_0(r_c/r)$. The numbers indicate v_z/v_o . A line parallel to the observing direction intersects these surfaces once, twice, or not at all.

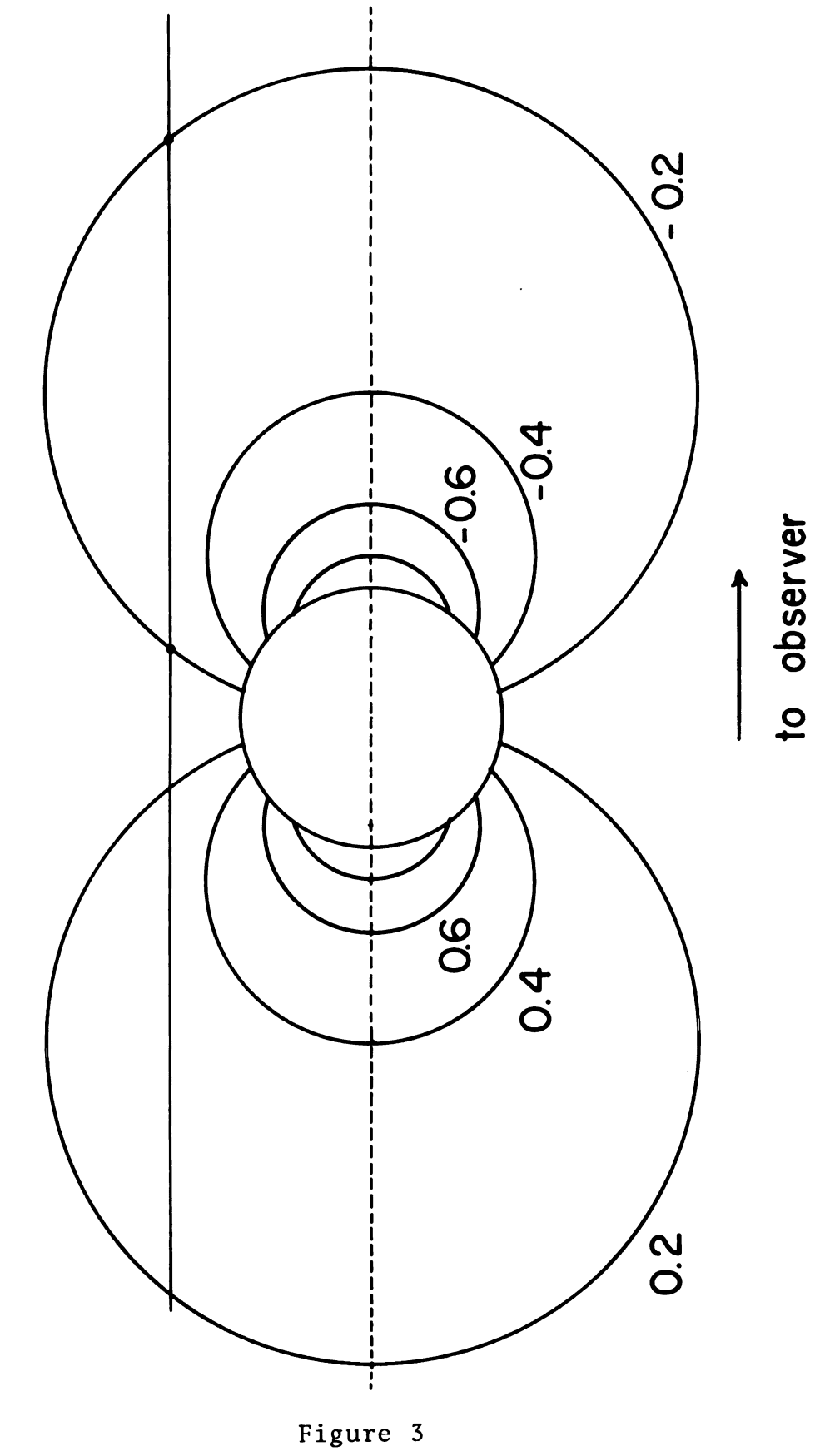


Figure 4. The straight line defined by the observer and the center of the star is the z axis, with its origin at the center of the star and the positive direction away from the observer. The intersection of the photospheric radius r_{c} and the line with impact parameter p has abscissa z_{c} . For each sphere of radius r, there are two surfaces of constant line of sight velocity, equal to $\pm v_{z}$, that have tangents at the intersection points parallel to the z axis; those intersections have abscissas z'_{d} and z''_{d} . z_{e} is the abscissa of the intersection of the line with impact parameter r_{c} and the sphere of radius r on the negative side of the z axis.

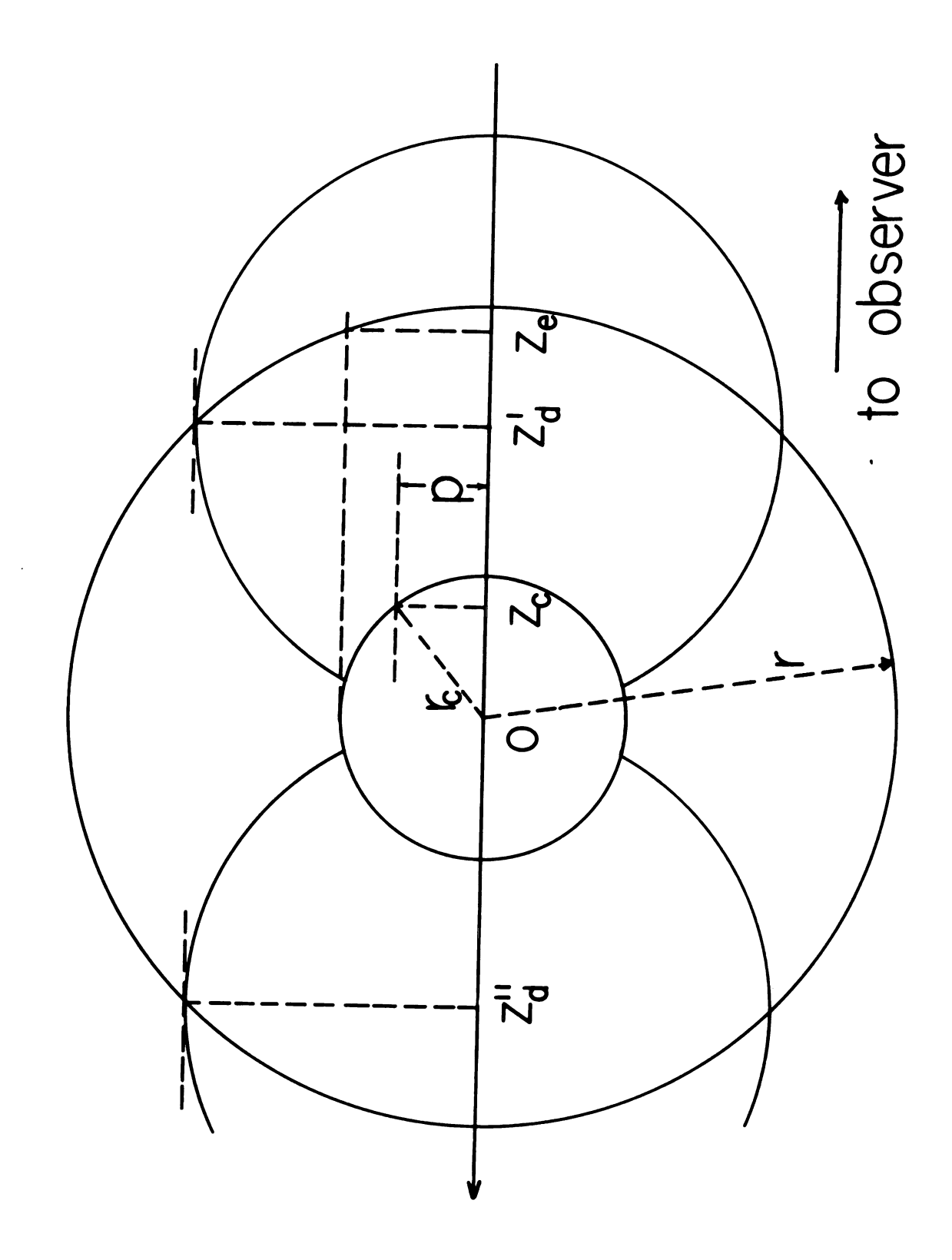


Figure 4

Figure 5. The star core, and a constant velocity surface and its intersection with a constant p line (horizontal dashed) are shown. The intersection closest to the observer has abscissa z_1 , the farthest, z_2 . On top there is a graph showing the optical depth as a function of z. The values of the auxiliary functions γ_1 and γ_2 in the different regions are given.

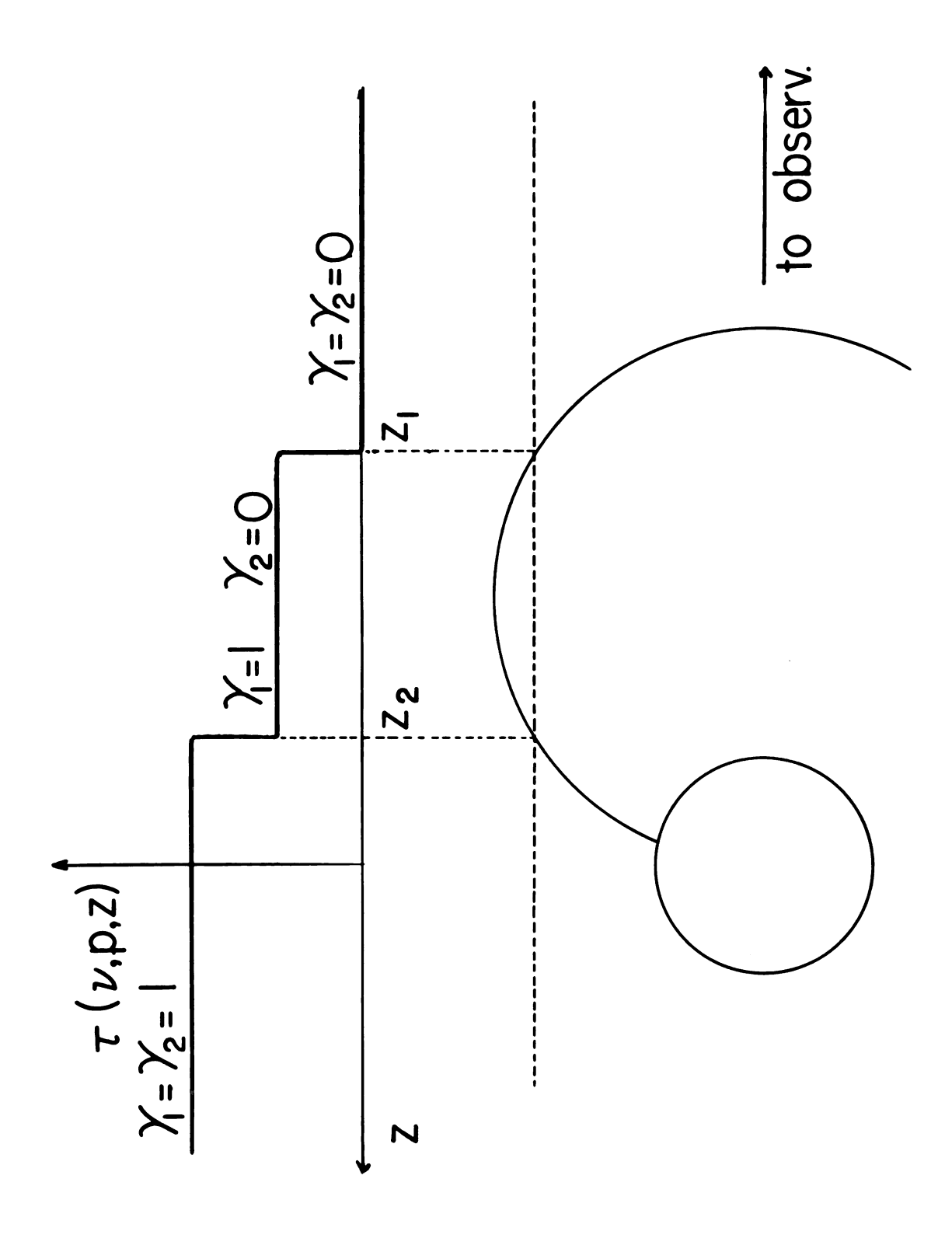


Figure 5

of τ for a case with two intersections of equal τ_i is shown in Figure 5. Evaluating the derivative in equation (II-14) along a line of constant p gives

$$\left(\frac{\partial x}{\partial z}\right)p, v = \frac{v_0}{c} \frac{\partial}{\partial z}\left[\frac{v(r)}{r} z\right] = \frac{v_0}{c}\left[\frac{v(r)}{r} + z\left(\frac{1}{r} \frac{dv}{dr} - \frac{v(r)}{r^2}\right)\frac{z}{r}\right] =$$

$$\frac{v_0}{c} \left[\frac{v(r)}{r} + (\frac{z}{r})^2 (\frac{dv}{dr} - \frac{v(r)}{r}) \right] = \frac{v_0}{c} \left[(1 - \mu^2) \frac{v(r)}{r} + \mu^2 \frac{dv}{dr} \right]. \quad (II-16)$$

In evaluating the different τ_i 's in equation (II-14) for use in equation (II-15), we can consider two extreme cases in equation (II-16). If our line of constant p passes through the center of the star, the optical depth that we will be determining is the optical depth in the radial direction. For p = 0, z = -r, $\mu = 1$

$$\tau_{\mathbf{r}} = \frac{k_{\ell}(\mathbf{r})}{\frac{v_{0}}{c} \left| \frac{d\mathbf{v}(\mathbf{r})}{d\mathbf{r}} \right|}, \quad \mathbf{r} = -\mathbf{z}$$
 (II-17)

Note that it is the optical depth as measured at location r toward the external observer in the radial direction. If instead, we take $v = v_0$, the intersection of the p = constant line with the surface of constant v_z (= 0), will be on the z = 0 axis (μ = 0), giving the optical depth in the tangential direction, perpendicular to τ_r

$$\tau_{t} = \frac{k_{\ell}(r)}{\frac{v_{0}}{c} \left| \frac{v(r)}{r} \right|}.$$
 (II-18)

The optical depth in the direction \hat{n} , making an angle α = \cos^{-1} μ with the radial direction is then

$$\tau(\hat{\mathbf{n}}) = \frac{k_{\ell}(\mathbf{r})}{\frac{v_{0}}{c}\left|(1-\mu^{2})\frac{v(\mathbf{r})}{\mathbf{r}} + \mu^{2}\frac{dv}{d\mathbf{r}}\right|}.$$
 (II-19)

Note that these τ 's were derived using the observer's direction as a preferred direction, but due to the symmetry of the problem they are completely general. For a power law velocity field like ours, (equation I-3), (II-17), (II-18), and (II-19) can be expressed as

$$\tau_{\mathbf{r}} = \frac{k_{\ell}(\mathbf{r}) \ \mathbf{r}^{\ell+1}}{v_{0} \frac{v_{0}}{c} \ell \mathbf{r}_{c}^{\ell}}, \qquad (II-20)$$

$$\tau_{t} = \ell \tau_{r} , \qquad (II-21)$$

$$\tau = \frac{\ell \tau_r}{\left|1 - \mu^2 (\ell+1)\right|} . \qquad (II-22)$$

The probability of a single emitted photon being in the solid angle $d\omega$ about \hat{n} , with frequency in the range x to x+dx is

$$\frac{d\omega}{4\pi} \phi(x) dx . \qquad (II-23)$$

Only the fraction $\exp[-\tau(\hat{n},x)]$ of those emitted will escape the surrounding region. Therefore the net escape probability is (Rybicki 1970)

$$\beta = \frac{1}{4\pi} \int d\omega \int_{-\infty}^{+\infty} dx \, \phi(x) \, \exp\left[-\frac{k_{\ell}(r)}{\left[\frac{\partial x}{\partial z}\right]p, \nu\right]} \int_{-\infty}^{x} \phi(x') \, dx', \quad (II-24)$$

where we have used the value of $\boldsymbol{\tau}$ from equation (II-14), and

then

$$\beta = \frac{1}{4\pi} \int d\omega \frac{\left| \left(\frac{\partial x}{\partial z} \right) p, \nu \right|}{k_{\ell}(r)} \left[1 - \exp\left(-\frac{k_{\ell}(r)}{\left| \left(\frac{\partial x}{\partial z} \right) p, \nu \right|} \right) \right], \quad (II-25)$$

or simply

$$\beta(r) = \frac{1}{2} \int_{-1}^{1} d \left[\frac{1 - \exp(-\tau)}{\tau} \right],$$
 (II-26)

where τ is given by equation (II-22). In the following, we shall often suppress the frequency ν and impact parameter p, which are always fixed during formal integration of S to obtain I, (although not when I is integrated to get the mean intensity \overline{J}). Also we may denote, for example, $(p^2+z^2)^{\frac{1}{2}}$ as r_1 , etc.

Substituting expression (II-15) into equation (II-5), we find for the case p > $\rm r_{\rm C}$

$$I(z) = S(r_1) \{1 - \exp[-\tau_1 \overline{\gamma}_1(z)]\}$$

$$+ S(r_2) \exp[-\tau_1 \overline{\gamma}_1(z)] \{1 - \exp[-\tau_2 \overline{\gamma}_2(z)]\}, (II-27)$$

where $\overline{\gamma}_i = 1 - \gamma_i$.

One must remember that either term in equation (II-27) may vanish if the intersection of the ray with the surface of constant z velocity falls outside the assumed outer radius of the atmosphere, r_m . For frequencies to the blue of line center, $|z_1|$ may be so large that r_1 exceeds r_m , in which case τ_1 is defined to be zero. For frequencies to the

red of line center (left half of Figure 3), z_2 may fall outside the atmosphere, and the term in $S(r_2)$ will be zero. (z_2 is always to the left, i.e. larger than z_1 by definition, as shown in Figure 5.)

For the case p < r_c , the cases z > 0 and z < 0 must be handled separately. In the former, there is no contribution from the photosphere, and the ray does not reach the observer, but is intercepted by the star. Such rays are perceived indirectly by the observer, because they affect the source function, however. For the case z > 0, the same equation (II-27) applies, with τ_2 still set equal to zero if $r_2 > r_m$; however, τ_1 must be set equal to zero, causing omission of the $S(r_1)$ term, if $r_1 < r_c$.

Finally, in the case $p < r_c$, z < 0, we have

$$I(z) = S(r_1) \{1 - \exp[-\tau_1 \overline{\gamma}_1(z)]\}$$

$$+ S(r_2) \exp[-\tau_1 \overline{\gamma}_1(z)] \{1 - \exp[-\tau_2 \overline{\gamma}_2(z)]\}$$

$$+ I_c \exp[-\tau_1 \overline{\gamma}_1(z) - \tau_2 \overline{\gamma}_2(z)], \qquad (II-28)$$

with the understanding that τ_2 vanishes if $r_2 < r_c$ or $r_2 > r_m$, and τ_1 vanishes if $r_1 > r_m$.

Mean Intensity and Source Function

The mean intensity itself is, of course, frequency dependent, and this dependence can differ considerably in the laboratory and fluid frames. From the work of Castor (1970) however, one expects the integral of the mean intensity over

the line profile,

$$\overline{J}(r) = \frac{1}{2r} \int_{-r}^{r} dz \int_{0}^{\infty} \phi(x) I[v, (r^{2}-z^{2})^{\frac{1}{2}}, z] dv, \qquad (II-29)$$

where x is defined in equation (II-10), to have an especially simple relationship to S. The integration over z in equation (II-29) actually represents an integral over $\mu;$ spherical symmetry has been used to rotate rays that would ordinarily pass through a common point on the shell of radius r so that they are instead parallel. We wish to manipulate equation (II-29) into an integral equation relating \overline{J} in the various layers and $I_{\text{C}}.$ It can then be combined with the excitation law for the two-level atom:

$$S(r) = \varepsilon B(T) + (1 - \varepsilon) \overline{J}(r) , \qquad (II-30)$$

where B is the Planck function evaluated at the line frequency and depends on the temperature T at radius r; ϵ is the ratio of collisional de-excitation rate to total de-excitation rate. The term in \overline{J} corresponds to the scattering contribution to the source function, while the term in B is produced by collisional excitation followed by radiative de-excitation (Mihalas 1970).

Returning to equation (II-29), the integration over ν is done first, leading to δ -functions that select the chosen layer at r and all other layers that couple to it radiatively. The results are best described in terms of Figure 4. The locus of the points in the constant line of sight velocity surfaces that have tangent parallel to the z axis can

be found from

$$\frac{\partial \mathbf{v}_{\mathbf{z}}}{\partial \mathbf{z}} = \frac{\partial}{\partial \mathbf{z}} \left[\mathbf{v}(\mathbf{r}) \ \frac{\mathbf{z}}{\mathbf{r}} \right] = 0 \tag{II-31}$$

$$\left(\frac{z}{r}\frac{dv}{dr} - \frac{zv}{r^2}\right)\frac{dr}{dz} + \frac{v}{r} = 0 , \qquad (II-32)$$

substituting dr/dz = z/r, and $dv/dr = -\ell v/r$ gives

$$\frac{z}{r} = \pm (\ell + 1)^{-\frac{1}{2}}.$$
 (II-33)

For a given r, the intersections with the locus are then

$$z''_d = -z'_d = r(\ell + 1)^{-\frac{1}{2}}.$$
 (II-34)

Also, clearly,

$$z_e = -(r^2 - r_c^2)^{\frac{1}{2}}.$$
 (II-35)

The integration in equation (II-29) is thus broken up at z_e , for the core cutoff, i.e. for $z < z_e$ p is smaller than r_c , while for $z > z_e$, p > r_c or z > 0. We also separate the integration at z'_d and z''_d to distinguish the cases where the intersections are single or double. The results are: for $z'_d > z_e$

$$J(r) = S(r) \left[1 - \frac{1}{2r} \int_{-r}^{r} G(\tau) dz\right]$$

$$+ I_{c} \frac{1}{2r} \int_{-r}^{2e} dz \exp(-\tau_{2}) G(\tau)$$

$$+ \frac{1}{2r} \int_{-r}^{2'} ddz S(r_{2}) G(\tau) \left[1 - \exp(-\tau_{2})\right]$$

$$+ \frac{1}{2r} \int_{0}^{z''} ddz S(r_{2}) G(\tau) \left[1 - \exp(-\tau_{2})\right], \quad (II-36)$$

and for $z'_d < z_e$

$$J(r) = S(r) \left[1 - \frac{1}{2r} \int_{-r}^{r} G(\tau) dz\right]$$

$$+ I_{c} \left[\frac{1}{2r} \int_{-r}^{r} dz \exp(-\tau_{2}) G(\tau) + \frac{1}{2r} \int_{z'}^{z} dz G(\tau)\right]$$

$$+ \frac{1}{2r} \int_{0}^{z''} dz S(r_{2}) G(\tau) \left[1 - \exp(-\tau_{2})\right]$$

$$+ \frac{1}{2r} \int_{-r}^{z''} dz S(r_{2}) G(\tau) \left[1 - \exp(-\tau_{2})\right], \quad (II-37)$$

where $G(\tau)$ is given by

$$G[\tau(\mu)] = \frac{1 - \exp(-\tau)}{\tau}$$
 (II-38)

In equations (II-36) and (II-37), unsubscripted τ 's are evaluated at radius r and at μ = -z/r, while quantities with subscript 2 must be evaluated by finding the other intersection of the ray with a surface of the same line of sight velocity, as in Figure 5. It should be noted that

$$d\beta = G(\tau) \frac{dz}{2r} , \qquad (II-39)$$

is the increment of escape probability.

When equations (II-30), (II-36) and (II-37) are combined, there follows an integral equation for S(r) of the form

$$S(r) \left[\frac{\varepsilon}{1 - \varepsilon} + \beta(r) \right] - \frac{1}{2r} \int_{-r}^{z'd} dz \ S(r_2) \ G(\tau) \left[1 - \exp(-\tau_2) \right]$$

$$- \frac{1}{2r} \int_{0}^{z''d} dx \ S(r_2) \ G(\tau) \left[1 - \exp(-\tau_2) \right]$$

$$= \varepsilon \ B/(1 - \varepsilon) + H(r) \ I_c , \qquad (II-40)$$

where
$$H(r)$$
 has different expressions, depending on z'_d and

where H(r) has different expressions, depending on z'_d and z_e for a given r. For $z'_d > z_e$

$$H(r) = \frac{1}{2r} \int_{-r}^{2e} dz \ G(\tau) \ exp(-\tau_2)$$
, (II-41)

and for $z'_d < z_e$

$$H(r) = \frac{1}{2r} \left[\int_{-r}^{z'd} dz \ G(\tau) \ \exp(-\tau_2) + \int_{z'd}^{z} dz \ G(\tau) \right]. \quad (II-42)$$

If we ignore the interconnections, letting τ_2 = 0 in equations (II-40), (II-41) and (II-42), we obtain

$$S(r)\left[\frac{\varepsilon}{1-\varepsilon} + \beta(r)\right] = \varepsilon B/(1-\varepsilon) + \beta_{c}(r) I_{c}, \qquad (II-43)$$

where

$$\beta_{c}(r) = \frac{1}{2r} \int_{-r}^{z_{e}} dz \ G(\tau) ,$$
 (II-44)

and can be approximated by

$$\beta_{c}(r) = \frac{1}{2r} \int_{-r}^{-(r^{2}-r_{c}^{2})^{\frac{1}{2}}} dz \ G(\tau) \simeq W(r) \ \beta(r) , \qquad (II-45)$$

where W(r) is the dilution factor

$$W(r) = \frac{1}{2} \left[1 - \left(1 - r_c^2 / r^2 \right)^{\frac{1}{2}} \right], \qquad (II-46)$$

that is the probability of a ray emitted in a random direction striking the core. We must notice that in this approximation (τ_2 = 0), we recover in our equations (II-30) and (II-43) Castor's (1970) result.

The description of the method of solution of the integral equation (II-40) is outlined in Appendix B, and some approximations useful in limiting cases are discussed in Appendix C.

Radiation Force

If the density is $_{\rho}(\textbf{r})\text{,}$ the absorption coefficient may be written

$$k(\nu,p,z) = k_{\varrho}(r) \phi(x) = \sigma(r) \rho(r) \phi(x), \qquad (II-47)$$

which defines the cross section per unit mass, σ . Then the radiation force per gram is

$$a(r) = \frac{2\pi\sigma}{c} \int_{-1}^{1} \mu d\mu \int_{0}^{\infty} \phi(x) I(\nu, p, z) d\nu, \qquad (II-48)$$

where x = ν - ν_0 + β z r⁻¹ and μ = -z/r, and I(ν ,p,z) is given by equations (II-27) and (II-28). Castor (1974) has

derived higher order corrections to equation (II-48) embodying the effects of sphericity and finite thermal line width, but he recovers the intuitive result (II-48) in the extreme supersonic limit. For resonance lines we approximate (see equation II-13)

$$k_{\ell}(r) = \frac{\pi e^2}{mc} (gf) \frac{N_1}{g_1},$$
 (II-49)

and set ρ = N m_{av} where N is the number density of all ions and m_{av} their average mass in grams. If X_{ion} then stands for the fraction <u>by number</u> of all ions in the state under consideration, we write

$$\sigma = k_{\ell}/\rho = \frac{\pi e^2}{mc} (gf) \frac{X_{ion}}{g_1 m_{av}}. \qquad (II-50)$$

Substituting I into equation (II-48) we get for $z'_d > z_e$

$$a(r) = \frac{2\pi\sigma}{cr^{2}} \left[\int_{-r}^{z'd} z \, dz \, G(\tau) \left[1 - \exp(-\tau_{2}) \right] \, S(r_{2}) \right]$$

$$+ \int_{0}^{z''d} z \, dz \, G(\tau) \left[1 - \exp(-\tau_{2}) \right] \, S(r_{2})$$

$$+ I_{c} \int_{-r}^{z_{e}} z \, dz \, \exp(-\tau_{2}) \, G(\tau) \right], \qquad (II-51)$$

and for $z'_d < z_e$

$$a(r) = \frac{2\pi\sigma}{cr^{2}} \left[\int_{-r}^{z'} z \, dz \, G(\tau) \left[1 - \exp(-\tau_{2}) \right] \, S(r_{2}) \right]$$

$$+ \int_{0}^{z''} d \, z \, dz \, G(\tau) \left[1 - \exp(-\tau_{2}) \right] \, S(r_{2})$$

$$+ I_{c} \int_{-r}^{z'} d \, z \, dz \, G(\tau) \, \exp(-\tau_{2})$$

$$+ I_{c} \int_{z'}^{z} e \, z \, dz \, G(\tau) \, . \qquad (II-52)$$

Fortunately, the coefficients needed for the acceleration a may be calculated in a similar manner and at the same time as those needed to formulate integral equation (II-40). When we considered the disconnected approximation we also omitted terms in $S(r_2)$ for the force, so that both the source function and the algorithm for obtaining the force from it were different. This is not intended as representative of Kuan and Kuhi's approach, because they did not consider the force; also they took into account the possibility for double absorptions once S was found in the disconnected approximation. Here it would likewise be possible to use an approximate S but then perform the integrals in equations (II-51) and (II-52) exactly. This is not particularly more consistent than what we used for the disconnected case. Furthermore, the labor of finding the second intersection in a rigorous integration for the force is tantamount to doing the labor for the whole calculation. We therefore assume anyone considering this kind of calculation of the force would solve the whole transfer problem rigorously, and thus

our "disconnected approximation" for the force is appropriate as an example of leaving out interconnections.

Line Profile

The power emitted by the star plus envelope, per unit frequency is

$$F_{v} = 4\pi \int_{0}^{r_{m}} 2\pi \ p \ dp \ I(v,p,-\infty) \ . \tag{II-53}$$

In the case $r_c , we have$

$$I(\nu, p, -\infty) = S(r_1)[1-\exp(-\tau_1)]$$

+ $S(r_2) \exp(-\tau_1)[1-\exp(-\tau_2)]$, (II-54)

and in the case 0 the result is

$$I(v,p,-\infty) = S(r_1)[1-\exp(-\tau_1)]$$

$$+ S(r_2) \exp(-\tau_1)[1-\exp(-\tau_2)]$$

$$+ I_c \exp(-\tau_1 - \tau_2), \qquad (II-55)$$

where, as usual, either τ is set equal to zero if that intersection is absent. If we combine these and normalize by the unattenuated continuum intensity

$$F_c = I_c 4\pi \int_0^{r_c} 2\pi p dp = 4\pi^2 r_c^2 I_c$$
, (II-56)

we obtain

$$F_{v}/F_{c} = (I_{c} r_{c}^{2})^{-1} \int_{0}^{r_{c}} \{S(r_{1})[1-\exp(-\tau_{1})] + S(r_{2}) \exp(-\tau_{1})[1-\exp(-\tau_{2})] + I_{c} \exp(-\tau_{1} - \tau_{2})\} 2 p dp + (I_{c} r_{c}^{2})^{-1} \int_{0}^{r_{m}} \{S(r_{1})[1-\exp(-\tau_{1}) + S(r_{2}) \exp(-\tau_{1})[1-\exp(-\tau_{2})]\} 2 p d p.$$
 (II-57)

CHAPTER III

RESULTS OF THE COMPUTATIONS AND COMPARISON WITH OBSERVATIONS

The Model Parameters

We have carried out the calculations with some attention to actual dimensional quantities relevant to stars and QSOs, but will express most of our results in terms of the following dimensionless parameters: the exponent & already defined, the ratio RR = r_m/r_c (outer envelope radius)/(core radius), the maximum integrated optical depth τ_o in the radial direction, and the values of ϵ and B/I $_c$. As the line opacity is proportional to the number of ions in the state under consideration, combining equations (I-4), (II-13), and (II-20) we obtain

$$\tau_r \propto r^{2\ell-1}$$
 . (III-1)

In the case $\ell=\frac{1}{2}$, $\tau_r(r)$ is constant and equal to its maximum, τ_0 . In the case $\ell=1$, $\tau_r(r)$ is linear in r, and hence attains its maximum τ_0 at $r=r_m$. This points up the tendency of decelerated flows to be more dependent on cutoffs at large r than accelerated ones. Almost all the runs were done with RR = 10, the choice of Kuan and Kuhi, and an economical one computationally. A few were done, however with RR = 3 and with RR = 15, so we can comment on the

effect of the cutoff. All our envelope models start right at the photosphere, where $v = v_0$.

Kuan and Kuhi (1975) applied their model to the case of P Cygni. They took the photospheric radius $r_{\rm C}$ equal to 10 $R_{\rm O}$ with an effective temperature of 30000 K and an absolute bolometric magnitude of -7.4. This value is probably too low, with the correct value closer to -10.4. The visual magnitude $M_{\rm V}$ is about -7.4 (DeGroot 1973), and the bolometric correction -3 (Allen 1973). Consequently the radius should be larger than 10 $R_{\rm O}$. We took this last value for most of our runs, but it is possible to use the results given in the graphs for sets of stellar dimensions and rates that differ from the ones we used in computing them, provided the new sets keep constant the fundamental parameters like $\tau_{\rm O}$, which is given by

$$\tau_{o} = \frac{\pi e^{2}}{mc} f_{ij} \frac{\chi_{ion} \dot{M}}{4\pi m_{av}} \frac{c (RR)^{2l-1}}{v_{o}^{2} v_{o}^{l} r_{c}};$$
 (III-2)

where \dot{M} is the mass loss rate. In all our computations we used \dot{M} = 1.06 10^{-7} solar masses/year and v_0 = 3000 km/s. The scaling law for the radiative acceleration is given below.

Source Function

The source function generally exhibits a sever attenuation with radius, as is appropriate for a very extended atmosphere, unless ε and B are large. When $\varepsilon\tau_0$ is large, then S \simeq B. In the disconnected approximation, it is easy

to show that (see Appendix C) for τ_{r} << 1

$$S \simeq \varepsilon B + W(1 - \varepsilon) I_C$$
, (III-3)

while, in the optically thick limit we have for $\tau_r >> 1$ and $r >> r_c$

$$S\left[\frac{\varepsilon}{1-\varepsilon} + \frac{1.177}{\tau_r}\right] \simeq \frac{1}{4\tau_r} \frac{r_c^2}{r^2} + \frac{\varepsilon B}{1-\varepsilon} , \quad \text{if } \ell = \frac{1}{2}. \quad (III-4)$$

$$S\left[\frac{\varepsilon}{1-\varepsilon} + \frac{0.6095}{\tau_r}\right] \simeq \frac{1}{4\tau_r} \frac{r_c^2}{r^2} + \frac{\varepsilon B}{1-\varepsilon}, \quad \text{if } \ell = 1. \quad (III-5)$$

The foregoing approximations support the idea that S falls rapidly with increasing radius, unless ϵB is large. These $1/r^2$ effects tend to dominate any of the finer differences that could be caused by the disconnected approximation, and they make graphs of the source function itself rather dull. Therefore we choose to exhibit only a few of the most significant cases. In Figure 6 we show the source function for the worst example we constructed for failure of the disconnected approximation. The difference in S is at most 0.28 in the logarithm, although it is still growing at r_m . On the basis of Kuan and Kuhi's remark that the approximation is good when the intensity from the core exceeds that from the envelope, one might expect to construct worse cases by making B large. However, we found in that case that if the envelope is thick the local B value dominates S

Figure 6. Comparison between the exact solution and the disconnected approximation for a star with RR = 10, $r_{c} = 10 \ R_{o}, \ \tau_{o} = 5, \ \epsilon = 0, \ \ell = 1. \ \text{In general, "exact solution" refers to including interconnections; the supersonic approximation is always used.}$

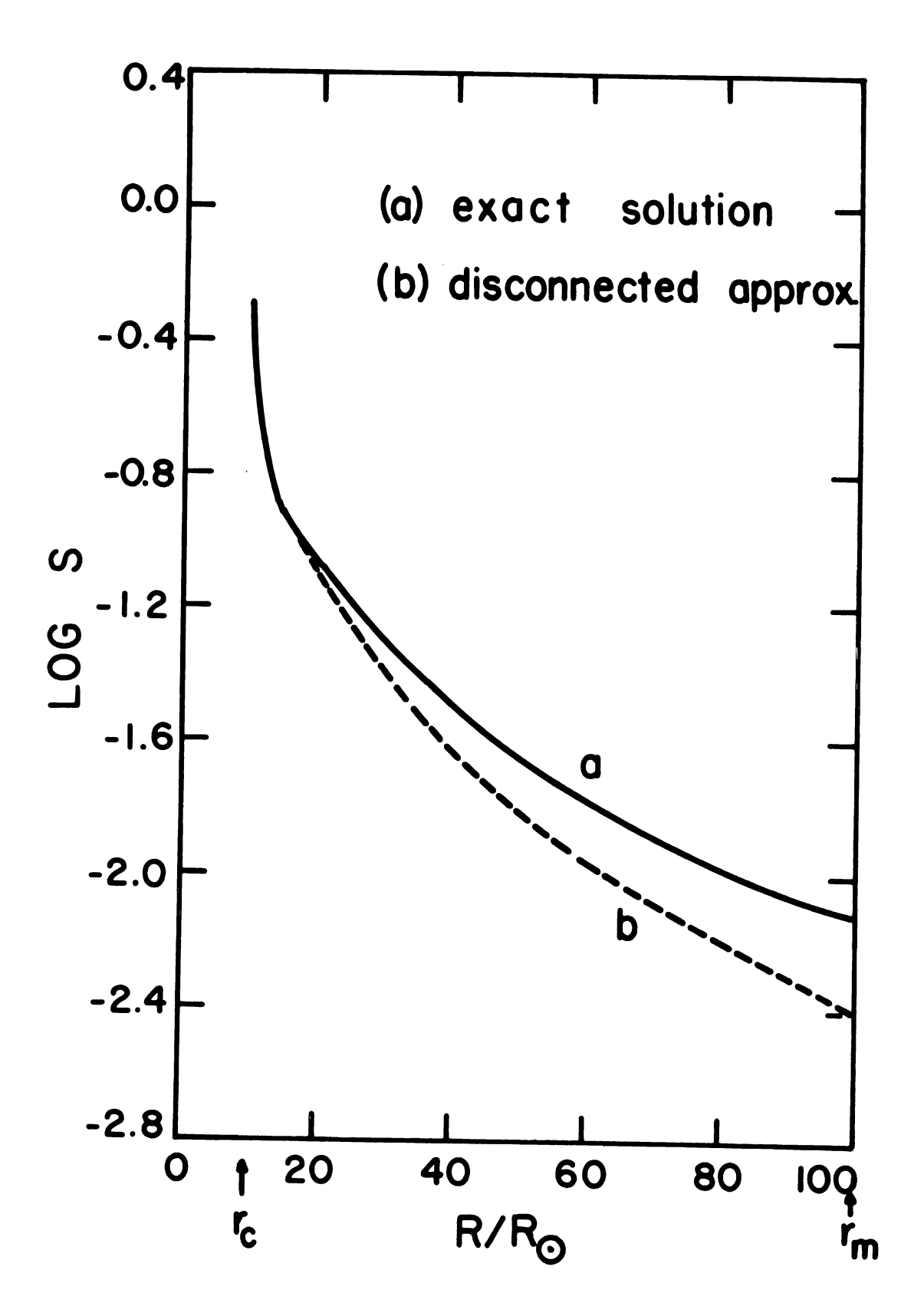


Figure 6

(but not in the force), while if it is thin, interconnections are obviously unimportant. It appears that cases with ε = 0 and intermediate optical depths are the worst; also we expect more discrepancy if r_m is increased. The reader should not consider that small changes in S where it is small are of no consequence at all, because there is a lot of volume and material out at large radius.

In several runs (not shown) with RR = 3, we found that toward the outer portion of the envelope the source function fell below that in the disconnected approximation. We traced this effect (which ran as high as 15%) to the discarding of absorption in inner layers in the disconnected approximation. (Note, however, that Kuan and Kuhi included such absorption in the underlying layer in their formal integration.)

The fact that the interconnections become more important at large RR suggests a bit of caution about the subordinate lines being independent of RR as long as it exceeds 10 (Kuan and Kuhi 1975). A change in S for resonance lines far out raises the ground state population for the subordinate lines.

In Figure 7 we show the effect of the outer cutoff on the source function in the exact solution. The three cases differ only in the value of RR, that is, we have added more material beyond r_m . We see that when we increase r_m , the value of the source function in the region common with the previous case increases. This is due to the fact that the

Figure 7. Effect of the outer radius on the source function.

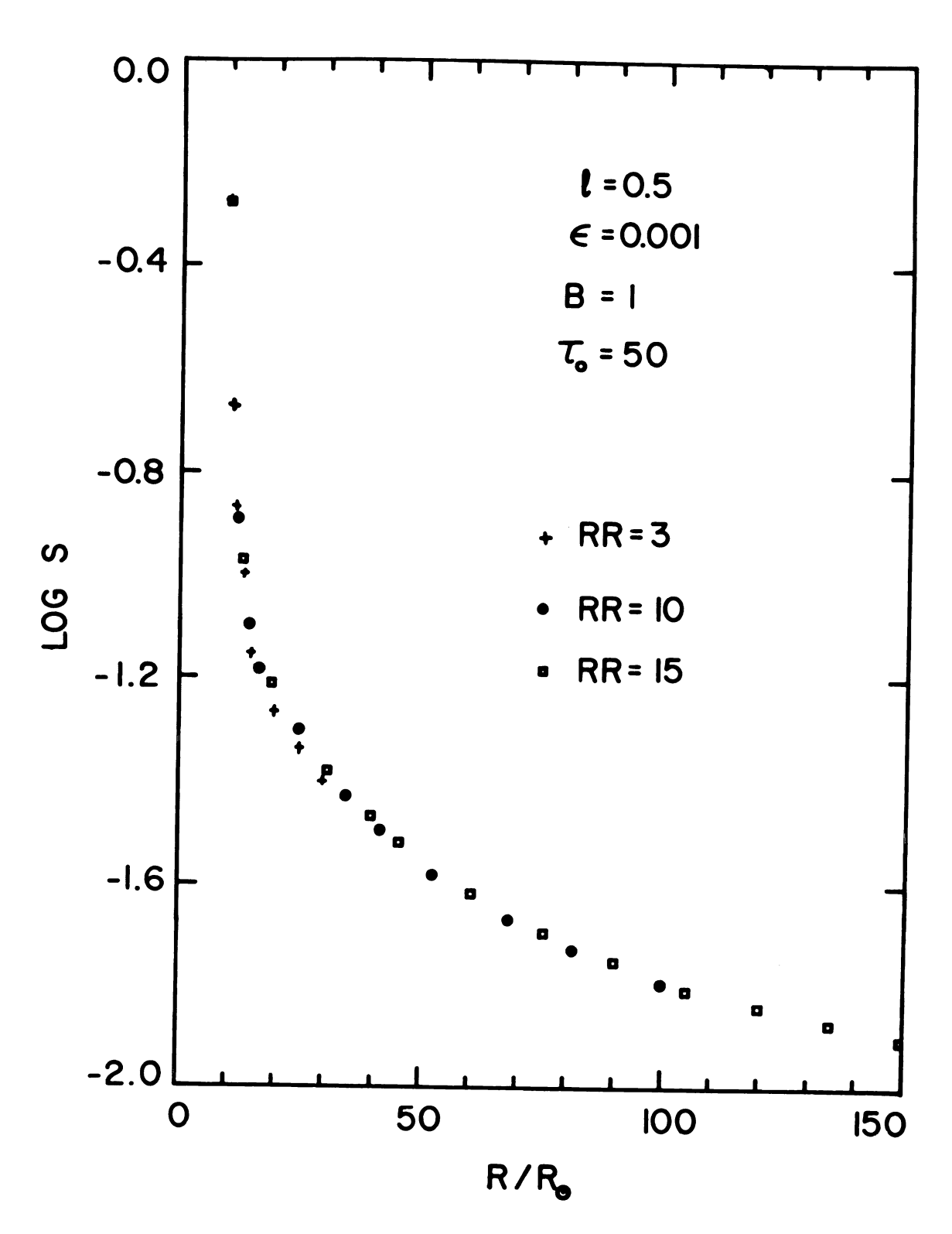


Figure 7

inner layers receive light from the outer ones, which increases the excitation. Remember that in the disconnected case the solution is completely local, i.e. for each layer it does not depend on how much material there is beyond that layer, (see equation II-43).

How does the optical depth affect the source function? We compare in Figure 8 three different cases, where all the parameters but the mass loss rate were kept constant, giving maximum optical depths of 0.1, 1, and 5.

In the region close to the core, the thinner the atmosphere the higher the value of the source function. If we refer to Figure 1, we see that in the case of point A, the surface able to interact with the atom at A, covers a large portion of the core, decreasing the amount of light received by the atom, and lowering the excitation. This effect may also be presented in the following fashion. Let us be reminded that the material on curve a, connecting point A in Figure 1 to the stellar surface has zero velocity of approach as seen by the material at A. Consider now a straight line from A to the stellar surface. If that line crosses the surface a, the optical depth will be large, resulting in a greatly diminished stellar intensity. It is obvious that making the atmosphere thicker will decrease S even more. When we are far from the core (point C in Figure 1) the interacting surface does not cover much of the core, but instead emits (in the case of Figure 8 scatters, $\varepsilon = 0$) light toward C, increasing the excitation.

Figure 8. Effect of the optical depth on the source function.

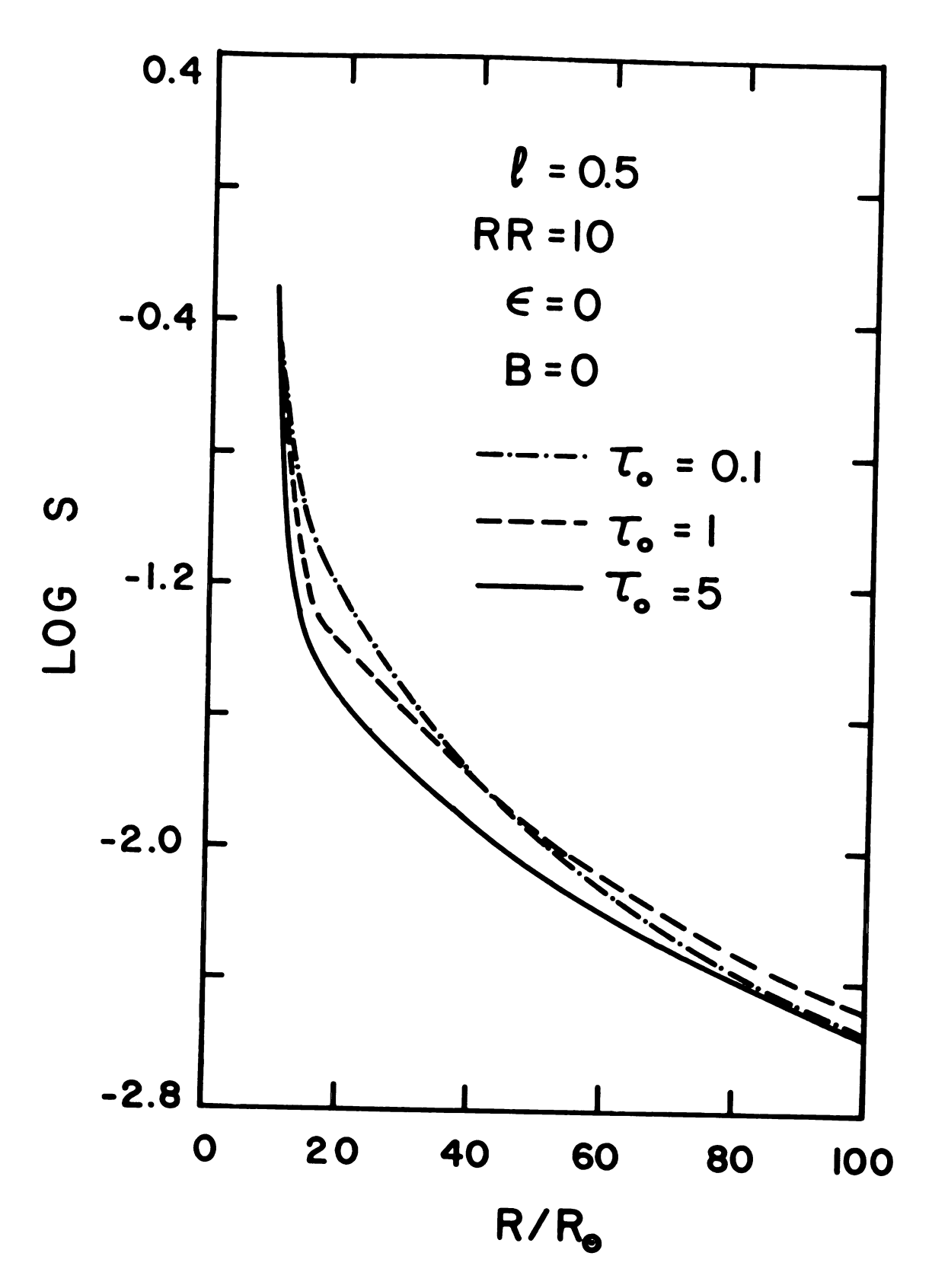


Figure 8

Radiative acceleration

We found it convenient to take out the strong r^{-2} dependence in the radiative acceleration by dividing by the acceleration of gravity GM/r^2 . For this purpose we chose physical parameters listed in the caption of Figure 9. It is possible to alter the combination in any way that preserves τ_0 and the product

$$C_F = I_c f_{ik} X_{ion} r_c^2/M$$
, (III-6)

where M is the mass of the star and X_{ion} the fraction of all ions in the gas in the form of the chosen ion. (We took mean ionic weight 1.2.) In all cases, we chose parameters corresponding to the C IV resonance line at 1550 Å, $f_{ik} = 0.286$, $I_c = 5.05 \times 10^{-3} \text{ erg cm}^{-2}$, and X_{ion} in the range 10^{-3} to 10^{-7} . The value of I_c corresponds to a 30000 K black body intensity at the C IV resonance line wavelength.

It is easy to convert to any case through equation (III-6). (The mass loss rate also enters the problem, but only in fixing τ_0 .)

The curious structure in the force law between the photosphere and 25 $R_{\rm O}$ is present in both the disconnected and regular cases. The dip is approximately where the cone of light from the core is tangent to one of the cones of maximum optical depth given by

•

Figure 9. The ratio of the radiative acceleration to that of gravity for the case shown in Figure 6. We assume a star of 10 solar masses, effective temperature 30000 K, τ_0 = 5, corresponding to X_{ion} = 10^{-6} , and other parameters as described in the text.

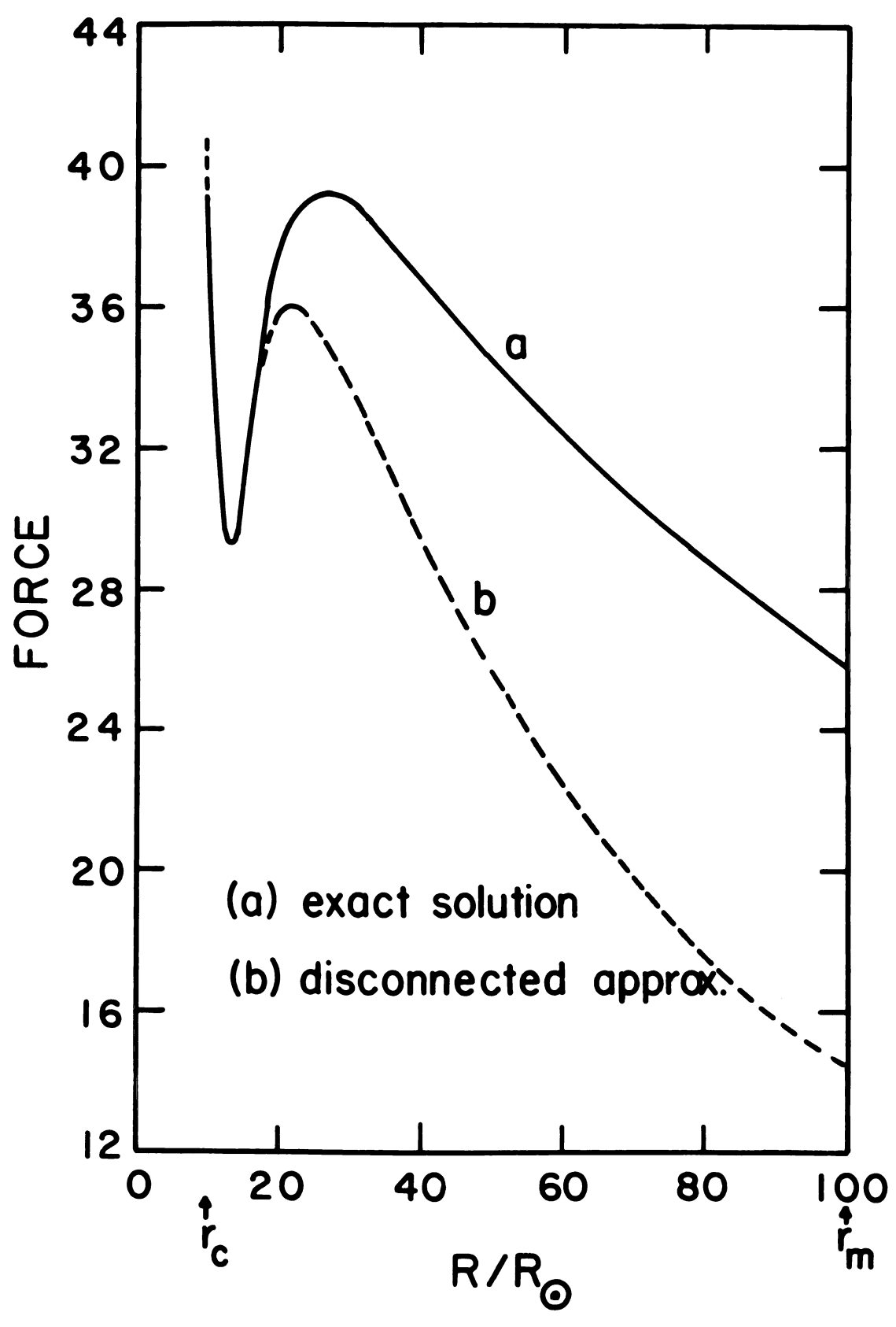


Figure 9

$$\mu = \pm \frac{1}{(\ell + 1)^{\frac{1}{2}}}.$$
 (III-7)

If the optical depth were independent of μ , we should obtain a r^{-2} dependence, that after dividing by the gravitational acceleration gives a flat curve. The drop for large r values is due to the increase of τ_r (remember that τ_r is linear in r for $\ell=1$).

The force in most of the atmosphere is highly altered in the disconnected approximation.

Figure 10 compares the force for atmospheres of various thicknesses. As expected, the force behaves essentially as r^{-2} in the optically thin case, although some of the peculiar structure due to the variation of τ with μ is present. Note that even in this case, the radiation force is much larger than the gravity force. Some saturation is present as τ increases beyond 1. It is worth noting that the mass loss rate or overall density was not changed in these runs, only the abundance of the ion with the resonance line. If, instead, the relative abundance were fixed and the total density increased, the average force would remain constant at very small optical depths, and then gradually drop as saturation was reached.

In Figures 11 and 12 we compare atmospheres with the same RR, ℓ , ϵ , density, and B, with two choices of X_{ion} and also with the interconnections turned off. In the first case, since ϵ_{T} is only 0.1, the Planck function is not able

Figure 10. Force law for the case RR = 10, r_c = 10 R_o , ϵ = 0, ℓ = 0.5, and three values of τ_o , as shown. In runs a, b, and c, X_{ion} was 5 x 10^{-6} , 10^{-6} , and 10^{-7} respectively.

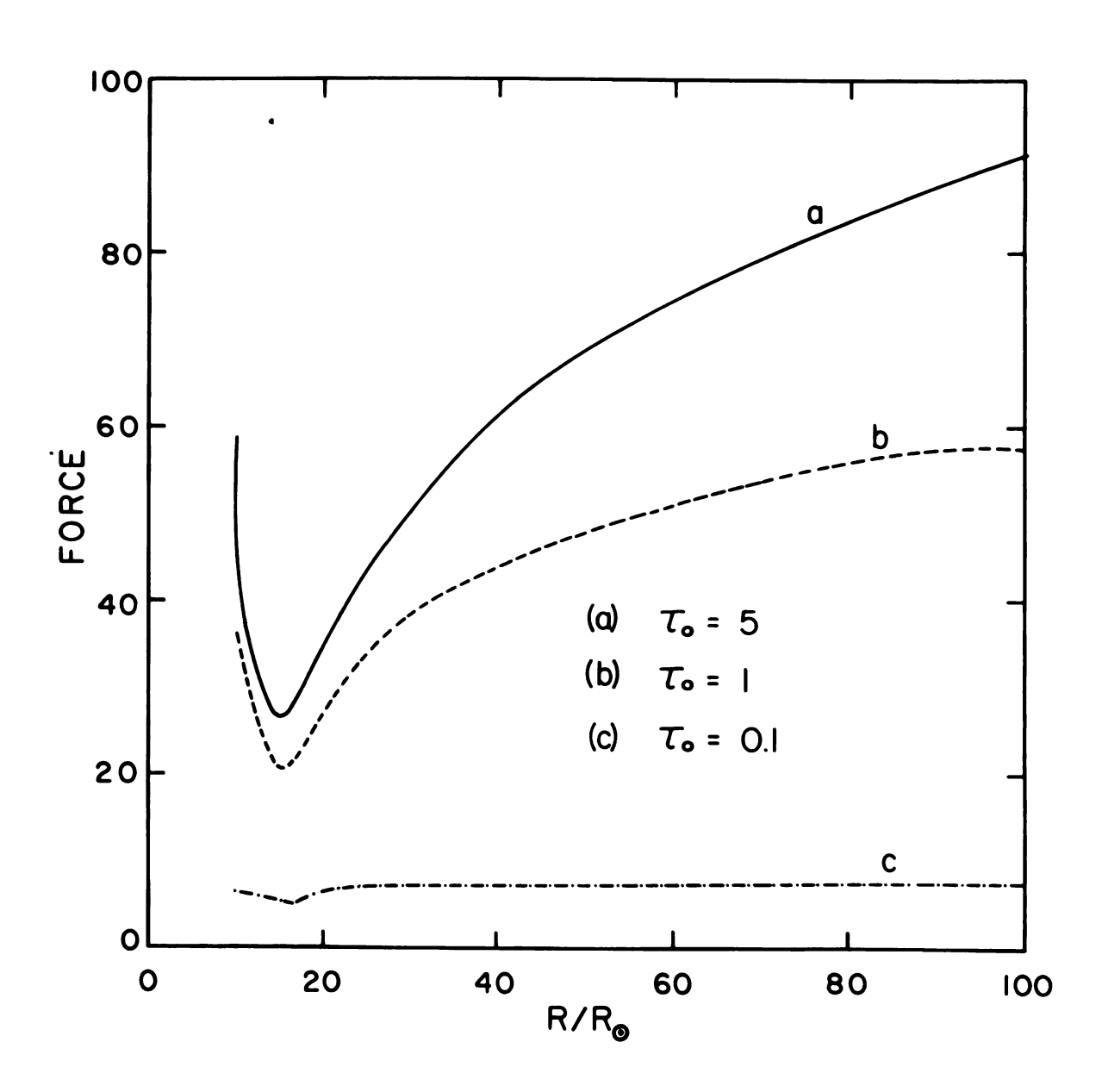


Figure 10

Figure 11. Comparison between the exact solution (solid curve) and the disconnected approximation of the force for a star with RR = 10, $r_c = 10 R_o$, $\tau_o = 100$, $\epsilon = 0.001$, $R_c = 10 R_c$, $R_c = 10^{-4}$.

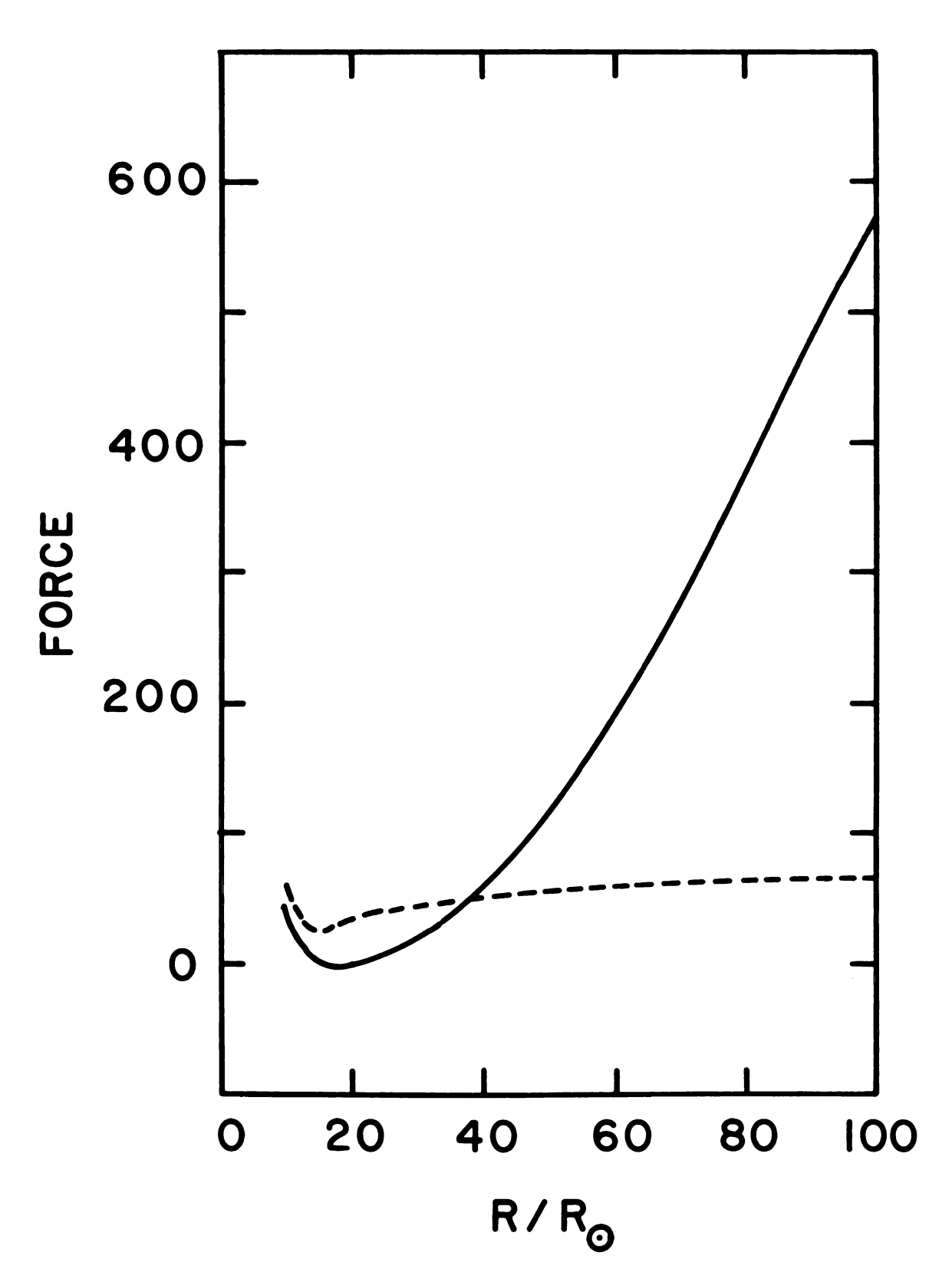


Figure 11

Figure 12. Comparison between the exact solution (solid curve) and the disconnected approximation of the force for a star with RR = 10, $r_c = 10 R_o$, $\tau_o = 1000$, $\epsilon = 0.001$, $R_c = 10 R_c$, $R_c = 10^{-3}$.

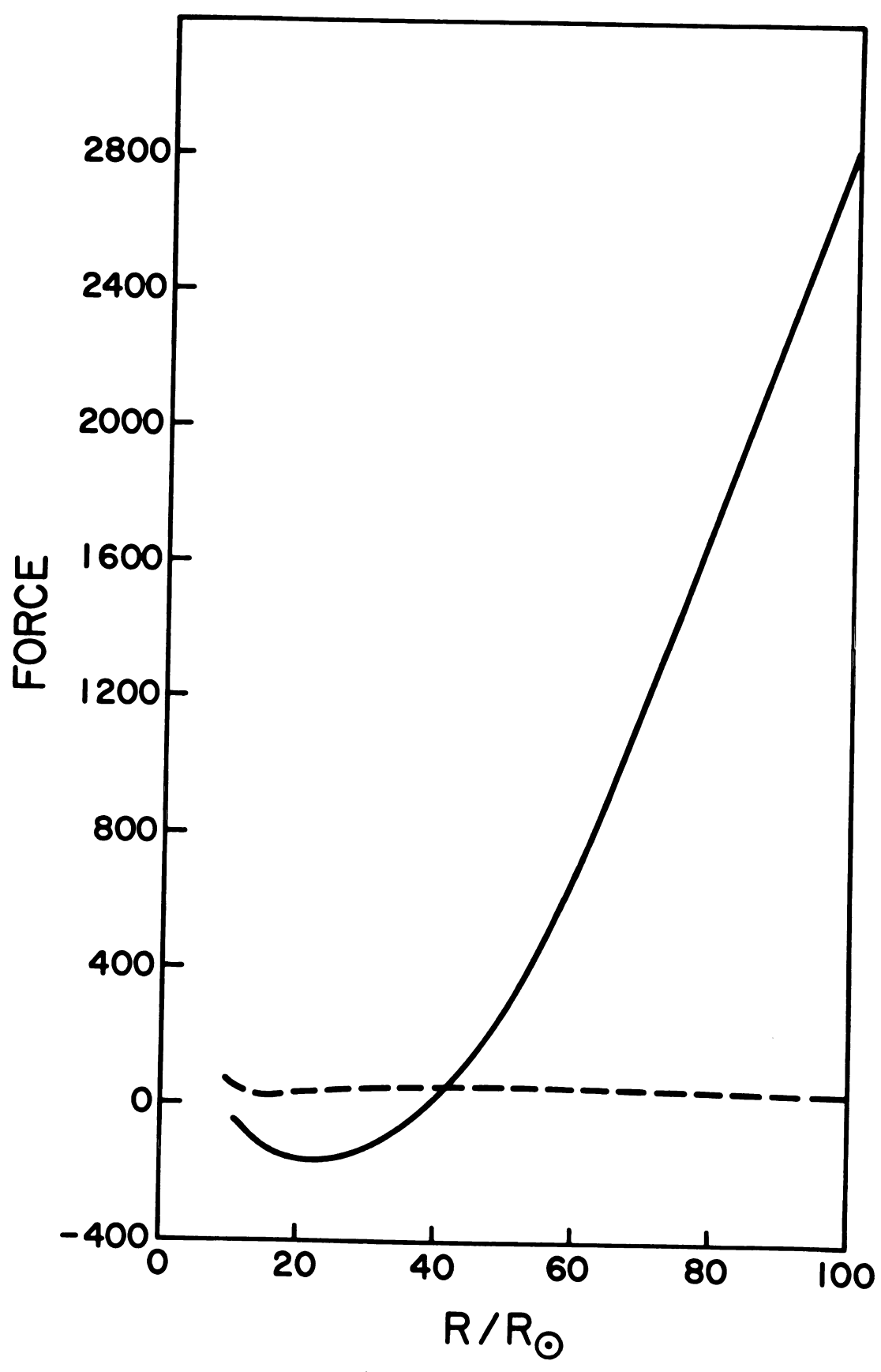


Figure 12

to do its maximum at pumping up excitation in the outer parts, while the second case is fairly extreme in that regard. In Figure 11, there is already evidence of some inward force on the inner layers due to radiation scattered and emitted in the outer layers. This is seen from the fact that near the star the force in the exact case falls below that in the disconnected case (although it is mostly outward). Evidently, the force from $I_{\rm C}$ still overcomes the inward force in this case.

In Figure 12 the inward force has actually dominated the outward near the star, and the disruptive effect of the interconnections is evident.

Line Profile

We studied a wide selection of cases with a view to determining: (a) how resonance lines behave as compared with the subordinate lines of Kuan and Kuhi, and (b) what the effect is on line profiles of making the disconnected approximation. We also tried to investigate what characteristic features of the line profiles could be used when fitting an observed profile with a synthetic one, to determine the parameters defining the velocity law, the conditions in the atmosphere and its dimensions.

As we said before, the agreement of the disconnected approximation with the exact solution for the line profile was good. Only in a few cases was the error in the equivalent width larger than a factor of 2.

We show in Figure 13 the line profiles obtained with

Figure 13. Comparison of the line profile in the exact solution (solid curve) and the disconnected approximation. The τ given is τ_0 . The abscissa is $(v-v_0)/\Delta v_m$ where $\Delta v_m = (v_0/c)v_0$.

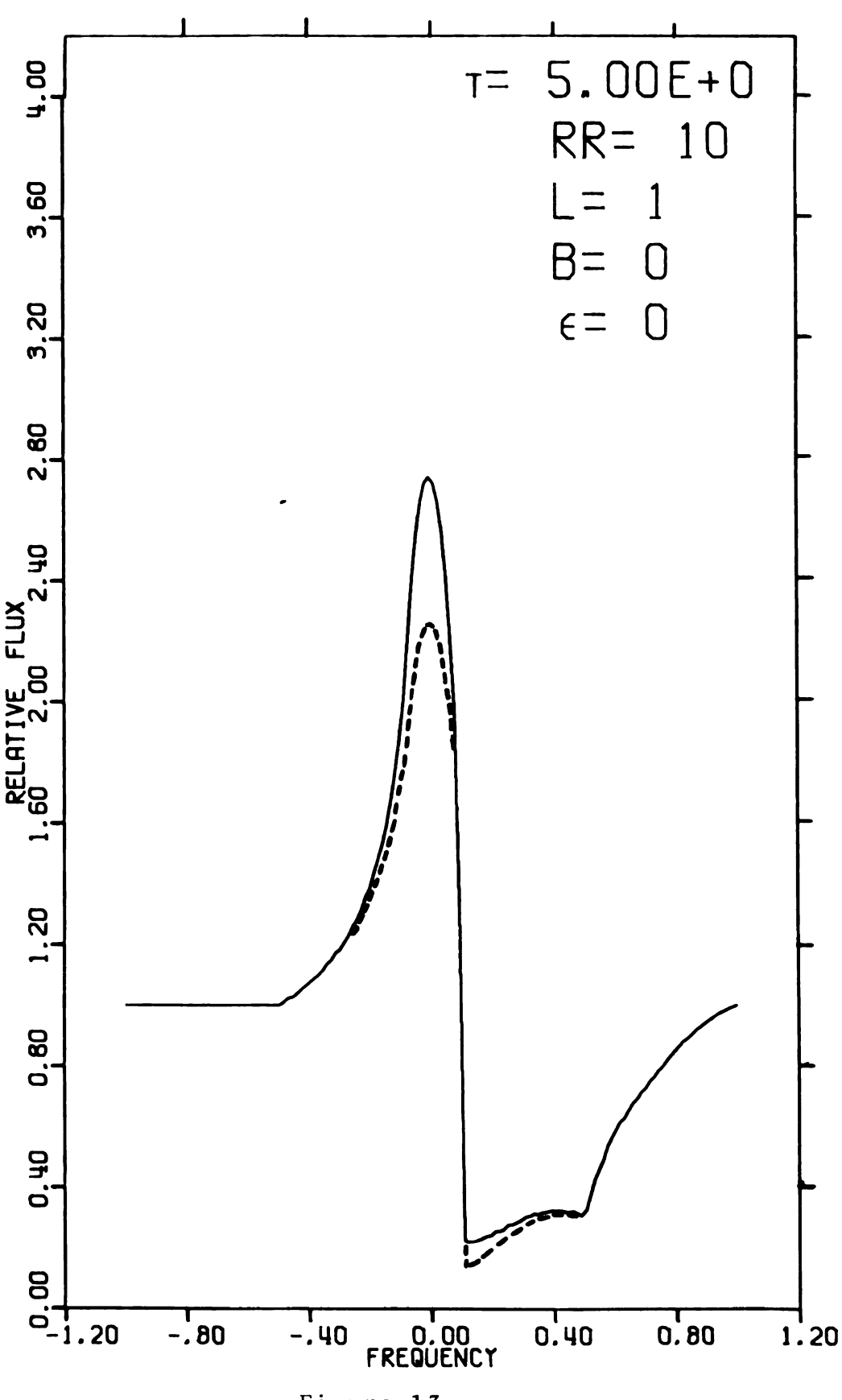


Figure 13

the disconnected approximation superimposed on the exact solution. This was one of the cases where we found important differences between the two line profiles.

As Kuan and Kuhi (1975) pointed out, the displacement of the shortward edge (point with frequency +1.0 in Figure 13) is determined by v_0 , the velocity at the photospheric radius. If v_0 is the central frequency, the maximum displacement in frequency is $\Delta v_{\rm m} = (v_0/c)v_0$. The displacement of the longward edge is given by their equation (14)

$$\Delta v_1 = -[\ell/(\ell+1)]^{\ell/2} [1/(\ell+1)]^{\frac{1}{2}} \Delta v_m$$
, (III-8)

from which we can determine the exponent L. This is the largest frequency for which the constant velocity surface is completely occulted by the star.

We observed, in most of our profiles, an absorption trough on the shortward side with very well defined limiting frequencies. When we move from the central frequency toward the blue side, a sudden drop occurs that we interpreted as reaching the frequency that corresponds to the first velocity surface completely contained within the cutoff radius \mathbf{r}_{m} . It can be shown that the frequency of the intensity minimum associated with this sudden drop is given by

$$\Delta v_2 = (r_c/r_m)^{\ell} \Delta v_m , \qquad (III-9)$$

from which we can determine the ratio r_m/r_c . When we are at this frequency or beyond, the light from the core will be absorbed by at least one layer of material.

The blue edge of this trough appears when we reach the frequency that corresponds to the velocity surface that starts to uncover the star core, that is $\Delta v_3 = -\Delta v_1$.

In Figure 14 we see how strongly the profile depends on the value of the cutoff radius $r_{\rm m}$. A run (not shown) with RR = 15 gave a peak of 5.39, and an equivalent width of -0.655. The equivalent widths given here and in the figure captions are defined as

$$EW = (2\Delta v_{m})^{-1} \int_{v_{0} - \Delta v_{m}}^{v_{0} + \Delta v_{m}} \frac{F_{c} - F_{v}}{F_{c}} dv , \qquad (III-10)$$

One might think that $r_m = 10 r_c$ is a reasonably large value and it is then possible to neglect the existence of material beyond that radius. From our results it appears that the effect of this additional material in the source function up to $10 r_c$ is small, but that it modifies the line profile, raising in some cases the peak value by a factor 1.5, and increasing the equivalent width (see Figure 14). We must note that Kuan and Kuhi (1975) did not find a similar effect for the subordinate lines.

Figure 15 shows two profiles calculated with different &. For both curves, the velocity at the star surface and the opacity at the outer radius were the same. It appears Figure 14. Comparison of two line profiles for atmospheres with τ_0 = 50, ϵ = 0.001, B(r) = $I_c(r_c/r)^{\frac{1}{2}}$, and ℓ = 0.5. Curve <u>a</u> corresponds to an atmosphere with RR = 10, (equivalent width (EW) = -0.410); curve <u>b</u> has RR = 3, (EW = -0.0739). Note that the case ℓ = 1 is expected to be more sensitive to the value of RR (see text).

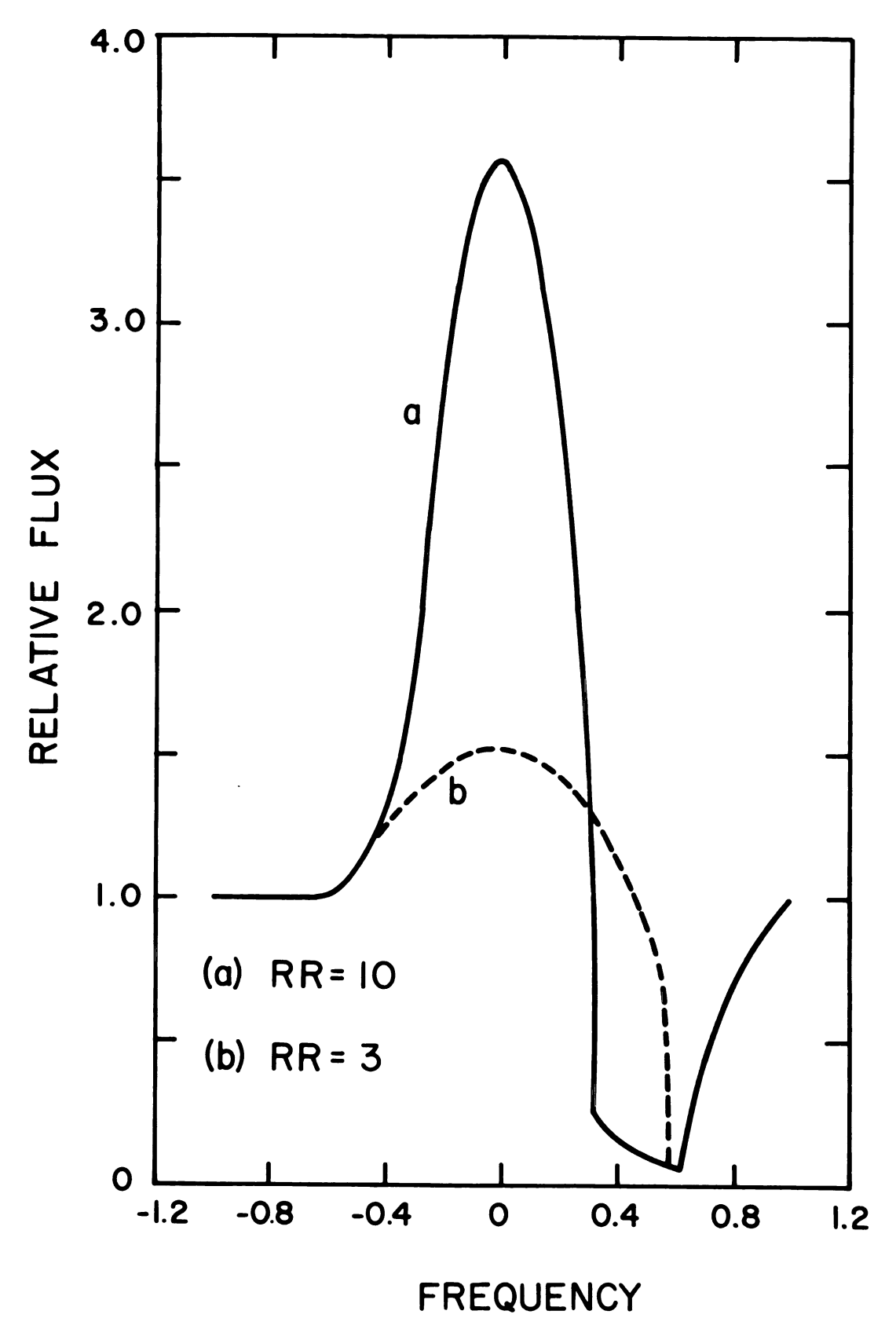


Figure 14

Figure 15. Effect of the exponent ℓ in the velocity law on the profile. Curve \underline{a} : $\ell=0.5$ (EW = 0.0086), curve \underline{b} : $\ell=1$ (EW = 0.0053). In both cases RR = 10, $\tau_0=1$, $\epsilon=0$.

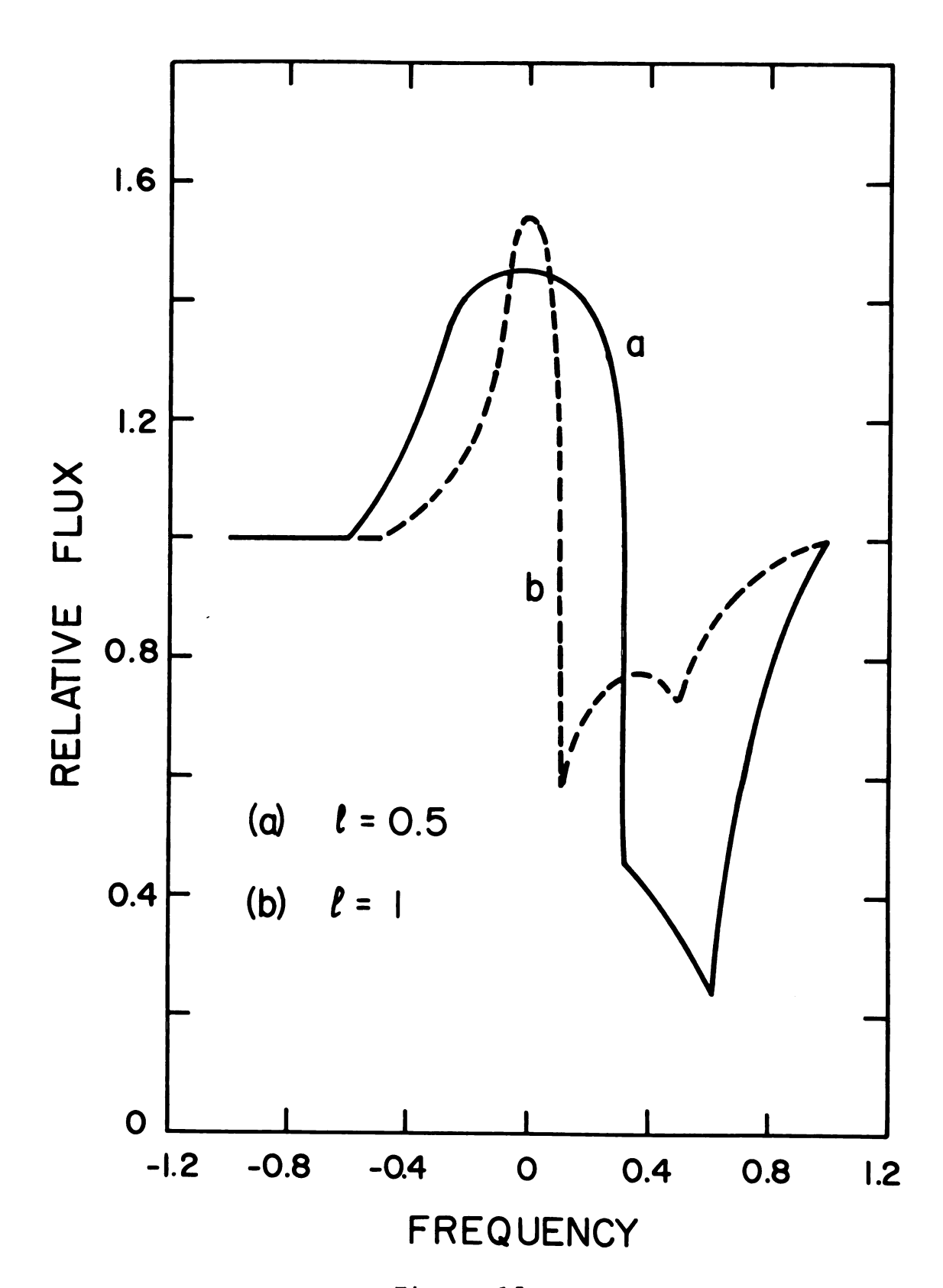


Figure 15

that larger & gives a sharper emission peak.

Figure 16 shows three atmospheres with different opacities. For τ_0 larger than 5 the saturation was so high that increasing τ_0 did not have any effect on the profiles (remember that in this case $\epsilon = 0$).

Unfortunately, most of the resonance lines have frequencies in the ultraviolet, which makes it impossible to observe them from ground based observatories. The recent access to rocket and satellite borne telescopes will ease this limitation.

We reproduce here some of the few available spectra from stars that are apparently ejecting mass, to see if the observational profiles resemble our synthetic ones.

Snow and Marlborough (1976) have obtained intermediate resolution (0.2 Å) UV spectra with the Copernicus satellite of 12 stars classified as Be or shell stars and several additional B stars. They found important assymetries in some resonance lines (especially the Si IV doublet at 1400 Å). We reproduce one of their figures in our Figure 17, that shows the Si IV λ 1400 profiles for several stars. The two vertical lines indicate the rest positions of the line centers. The error bars shown at the left represent the 2σ rms noise at the continuum level due to photon statistics. These profiles do not show the sharp drop-off that characterizes our synthetic profiles nor the flat bottomed absorption region.

Really, we cannot discard completely the decelerating

Figure 16. Profiles for three atmospheres with RR = 10, ϵ = 0, ℓ = 0.5, and τ_o as indicated. Curve <u>a</u>: EW = 0.0050, curve <u>b</u>: EW = 0.0086, curve <u>c</u>: EW = 0.0028.

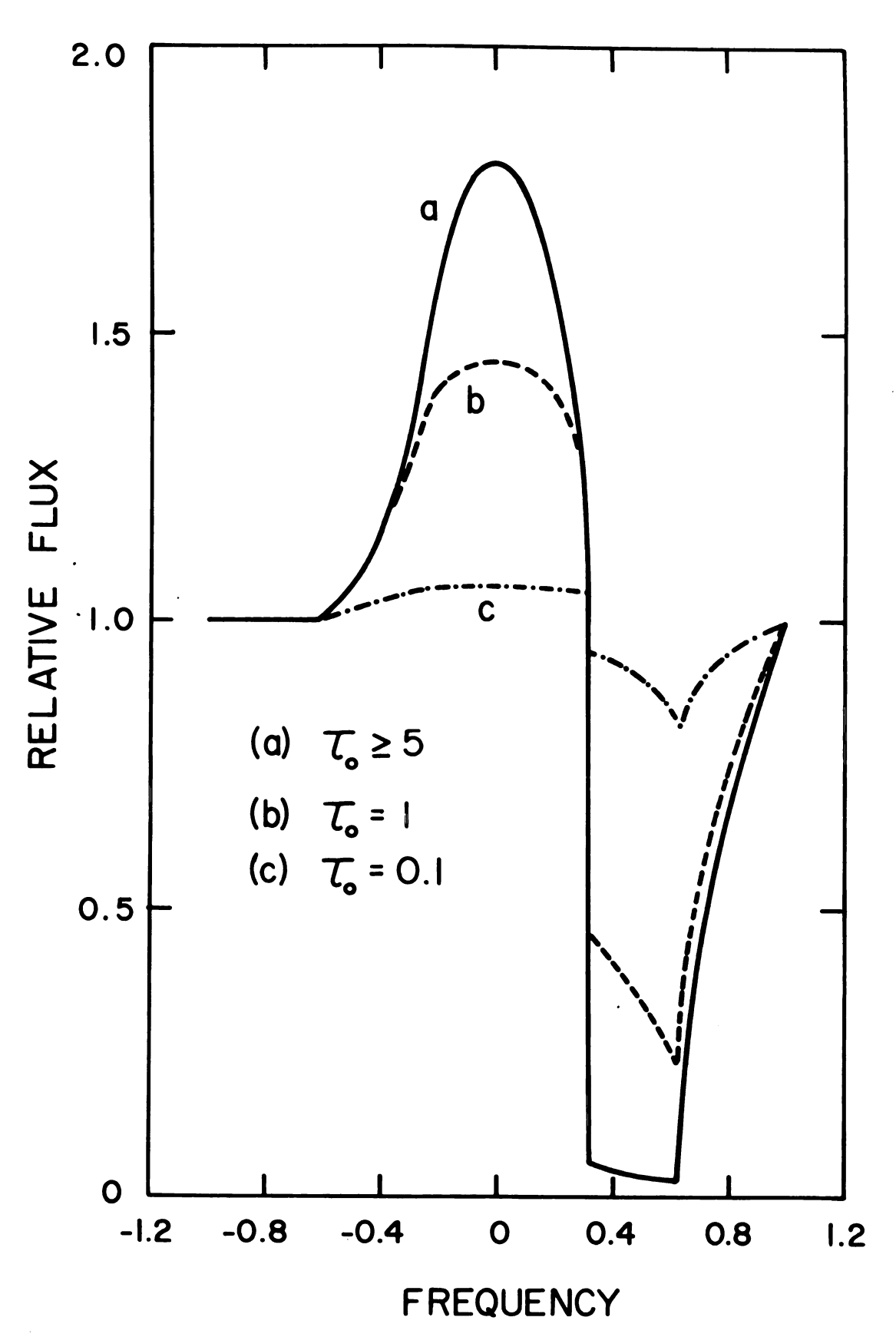
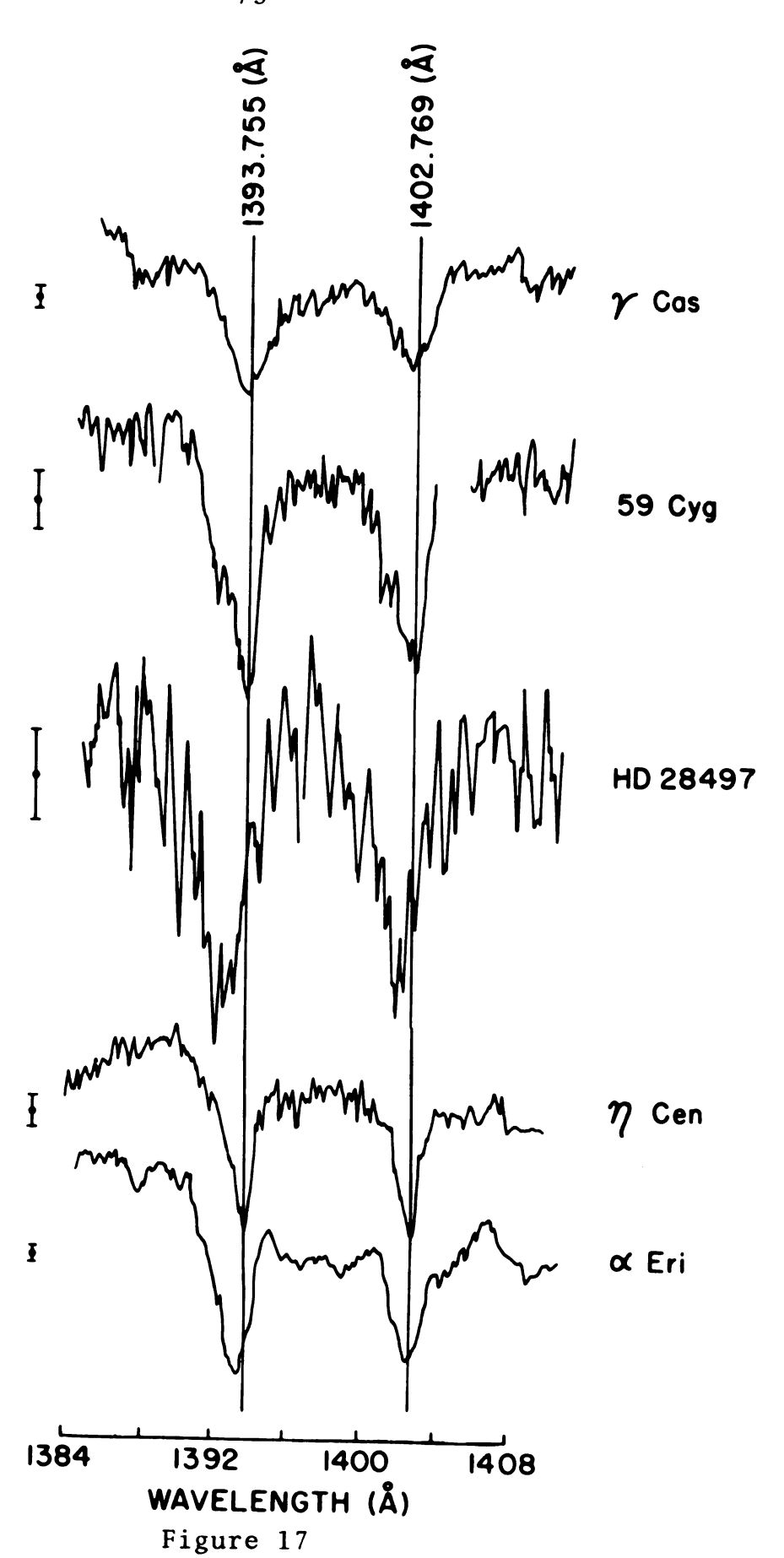


Figure 16

Figure 17. The Si IV λ 1400 profiles for several stars. After Snow and Marlborough (1976). By permission of The University of Chicago Press.



atmosphere model for this type of star, due to the possibility of rotational distortion of the profile. Snow and Marlborough (1976) studied the correlation between mass loss, temperature, and projected rotational velocity, and found that the stars showing mass ejection usually had high temperature and high rotational velocity. This indicates that the ultraviolet flux from the high temperature stars was not enough to accelerate the mass unless the rotation reduces the escape velocity. If the flow is not directed radially outward we cannot use our simple theory of the profiles.

Another set of observations with the Copernicus satellite are those of Hutchings' (1976). He studied several OB supergiants. We reproduce in our Figure 18 some of his scans of individual stars between 1165 and 1255 Å smoothed over 1 Å. They show the Si III λ 1206, Ly α , and the N V λ 1238,42 resonance lines. The C III λ 1175 is not a resonance line, but as the excitation potential is quite large (10.5 eV) and the lower level is a metastable one, our approximations are also valid for it.

None of the resonance lines show the features previously noted in our synthetic profiles. The C III line is closest to ours, especially in the star HD 188001. The apparent dissimilarity among the lines could be explained with a model in which groups of lines are formed in regions that are expanding at a different rate.

Hutchings computed the velocity excitation slope,

Figure 18. Upper: Copernicus scans of individual stars from 1165 to 1255 Å, smoothed over 1 Å. Center: unsmoothed mean spectrum of all stars in upper section, with continuum drawn in. Lower: mean of 11 scans of C III λ 1175 for P Cyg and ξ^1 Sco.

After Hutchings (1976). By permission of The University of Chicago Press.

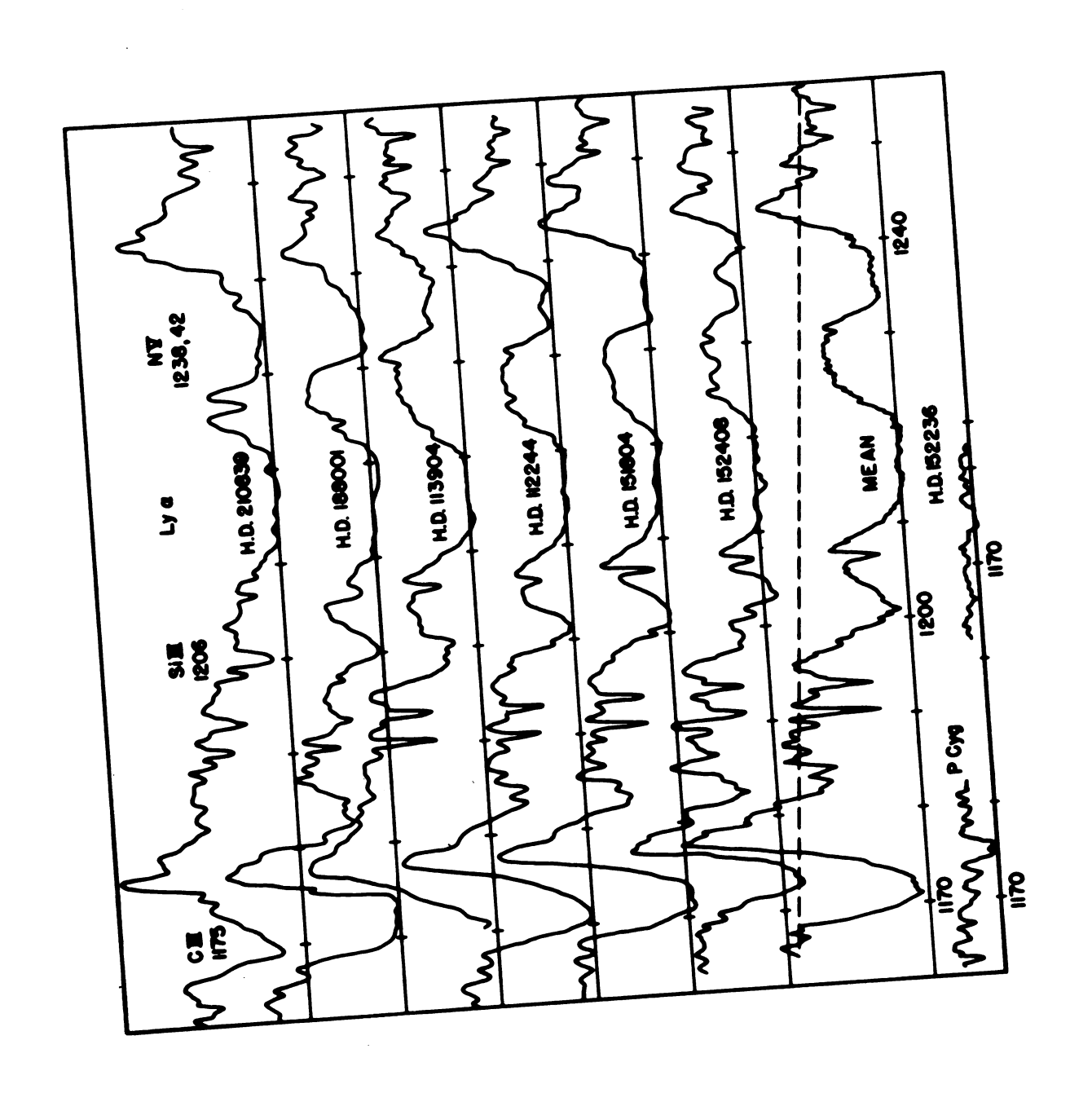


Figure 18

i.e. the slope of the velocity versus excitation potential curve, where each point is determined from a line in the spectrum. For HD 188001, he obtained a positive slope (taking velocities toward the observer as positive), that is: higher velocities in the regions of high excitation. This relation is not what he expected under his assumption that the velocity increased with radius, and he interpreted it as indicative of a large departure from Local Thermodynamic Equilibrium (LTE). But it could be explained simply by assuming a decelerating atmosphere as in our model.

Lamers and Morton (1976) studied the 04 star Zeta Puppis. They tried to explain the resonance line profiles with an accelerating atmosphere model. We reproduce the observed profiles in our Figure 19. The dotted lines are the observed intensities for different ions normalized to a maximum velocity $\mathbf{v}_{\infty} = 2660$ km/s, i.e. the maximum displacement in frequency from the line center is $(\mathbf{v}_{\infty}/c)\mathbf{v}_{0}$. The solid lines are their synthetic profiles. Just by inspection we see no similarities between the observed and our synthetic profiles. Apparently, this star does not have a decelerating atmosphere, at least in the region where the resonance lines are formed.

Finally, a strong candidate to apply our model is the QSO PHL 5200. We show in Figure 20 the C IV λ 1550 resonance line, based on the tracings from Scargle, Caroff and Noerdlinger (1970). Unfortunately there is no calibration available to allow us to determine the different

Figure 19. The dots represent the observed profiles of the resonance lines (normalized to $\rm v_{\infty}$ = 2660 km/s) of Zeta Puppis.

After Lamers and Morton (1976). By permission of The University of Chicago Press.

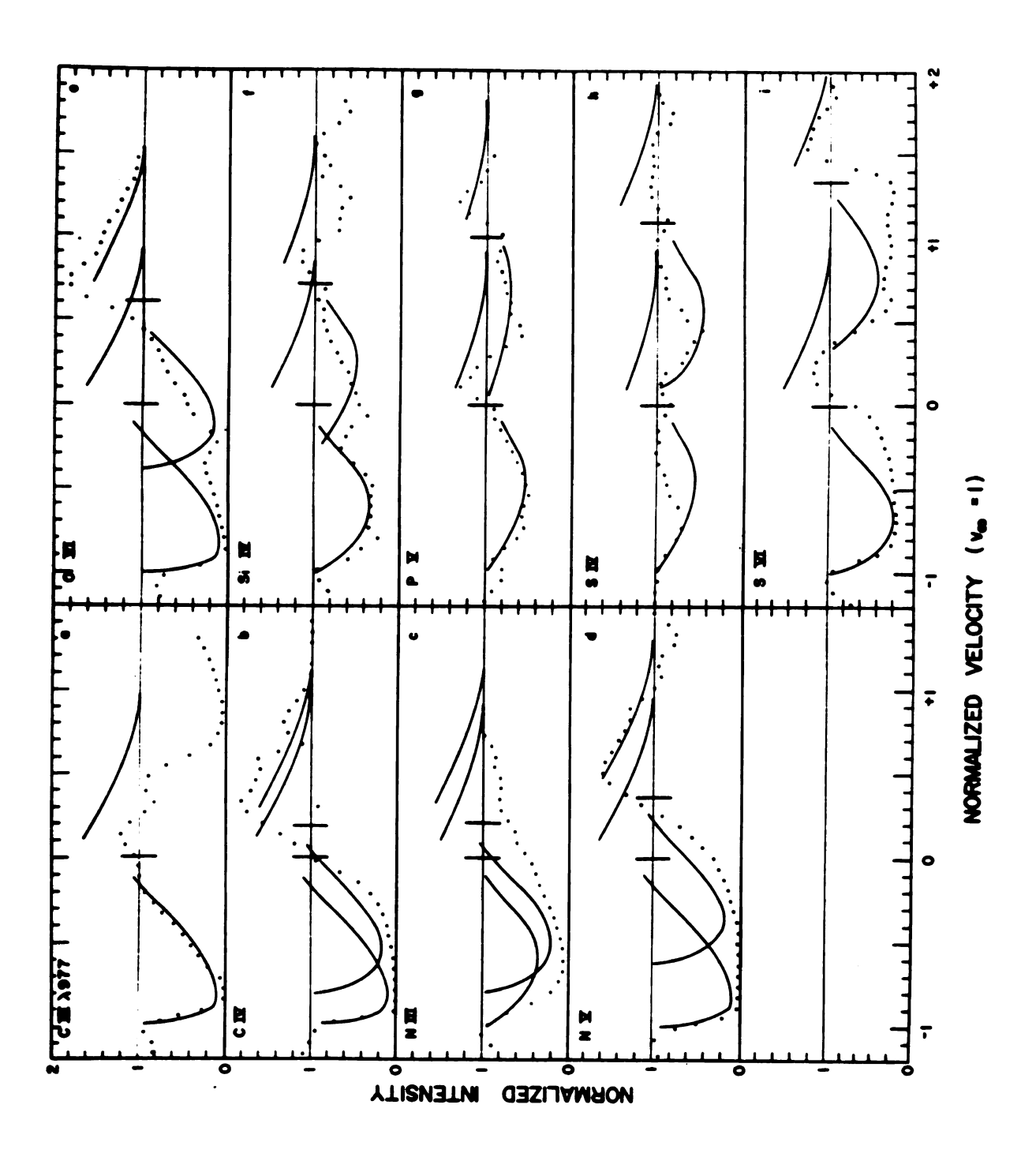


Figure 19

Figure 20. The C IV λ 1550 resonance line profile observed for the QSO PHL 5200.

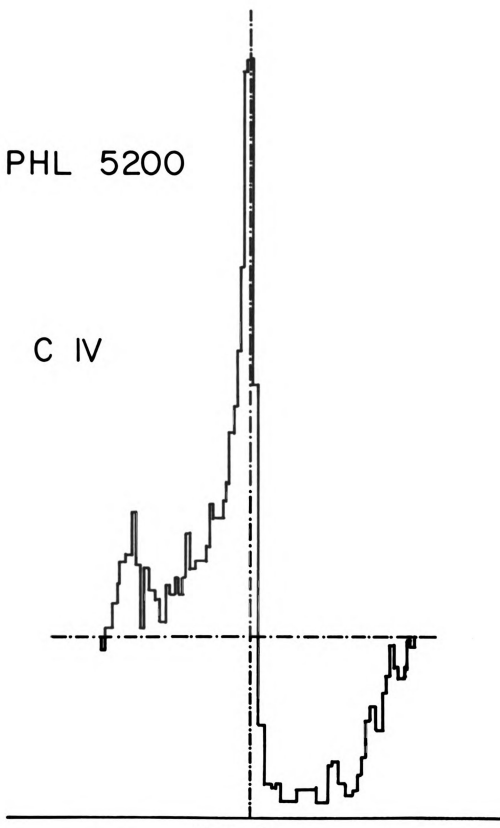


Figure 20

characteristic frequencies and from them the velocity law and dimensions. But it is obvious that the sharp drop and the absorption trough are quite similar to ours. The Si IV λ 1397 line shows a similar behavior. The secondary peak on the red side (left of Figure 20) corresponds to the Fe II λ 1608 line.

After this work was completed we became aware of the work of Grachev and Grinin (1976), who solved the expanding decelerating case for a somewhat different velocity field and only for ε = 0. They arrived at conclusions like ours about the QSO PHL 5200.

Image

Figures 21 to 24 show the products p $I_{tot}(p,-\infty)$ and p $I_r(p,-\infty)$ (curves with R's) versus p/r_m , where

$$I_{tot}(p,-\infty) = \int_{v_0-\Delta v_m}^{v_0+\Delta v_m} I(v,p,-\infty) dv$$
 (III-11)

$$I_{\mathbf{r}}(p,-\infty) = \int_{v_0^{-\Delta v_m}}^{v_0} I(v,p,-\infty) dv . \qquad (III-12)$$

These are intended to show the brightness variations one could attempt to look for with interferometry, speckle interferometry, or occultation by a companion or by the Moon. We choose wavelength bands intended to capture a reasonable amount of light and yet present as much contrast as possible for observation. We show only the few cases in

Figure 21. p I_{tot} and p I_r versus p/r_m for a star with RR = 3, τ_o = 50, ϵ = 0.001, B = I_c , and ℓ = 0.5.

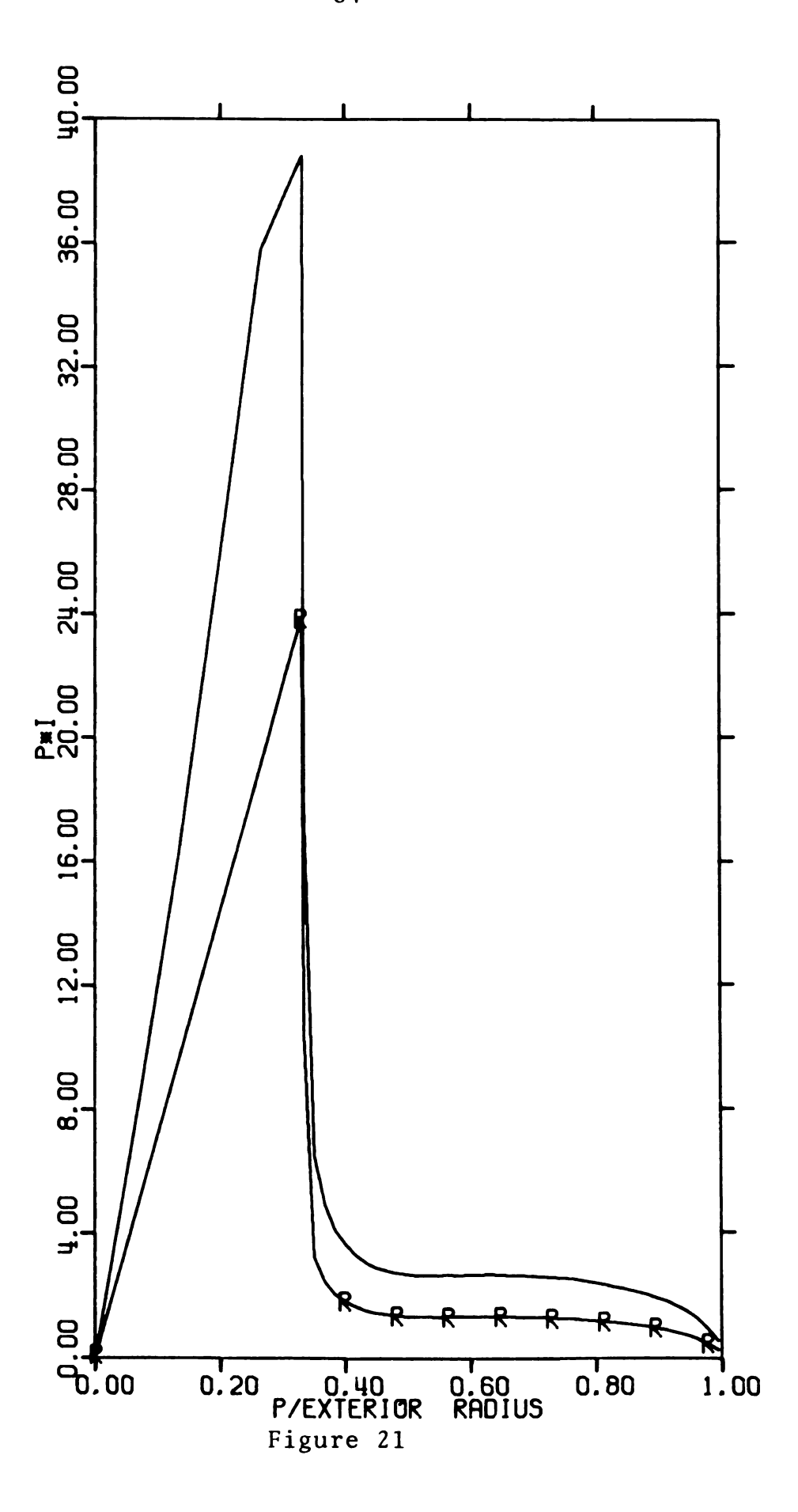


Figure 22. p I_{tot} and p I_r for a star with RR = 10, τ_o = 100, ϵ = 0.001, B = 5 I_c , and ℓ = 0.5.

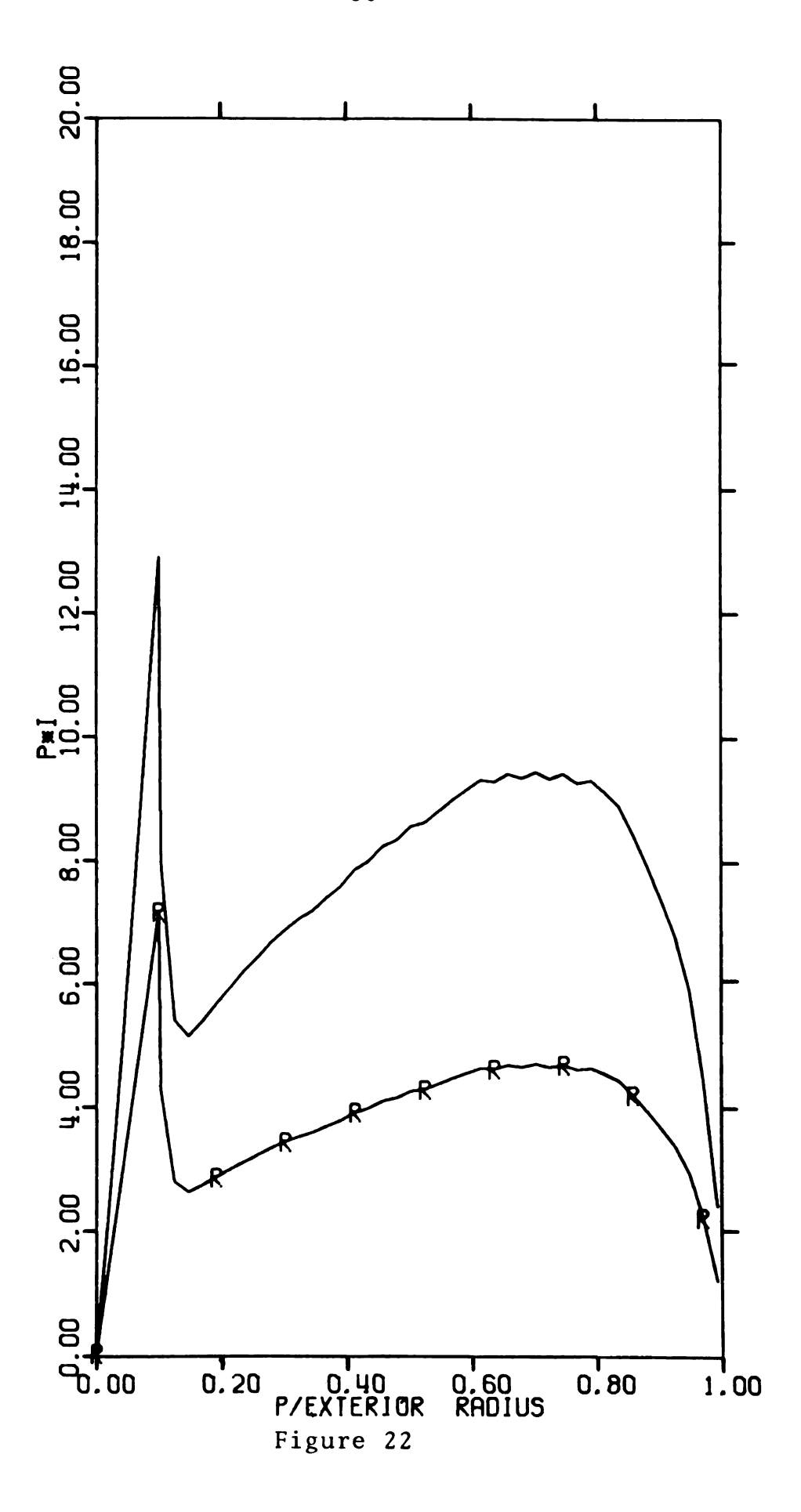


Figure 23. p I_{tot} and p I_{r} for a star with RR = 10, τ_{o} = 1000, ϵ = 0.001, B = 5 I_{c} , and ℓ = 0.5.

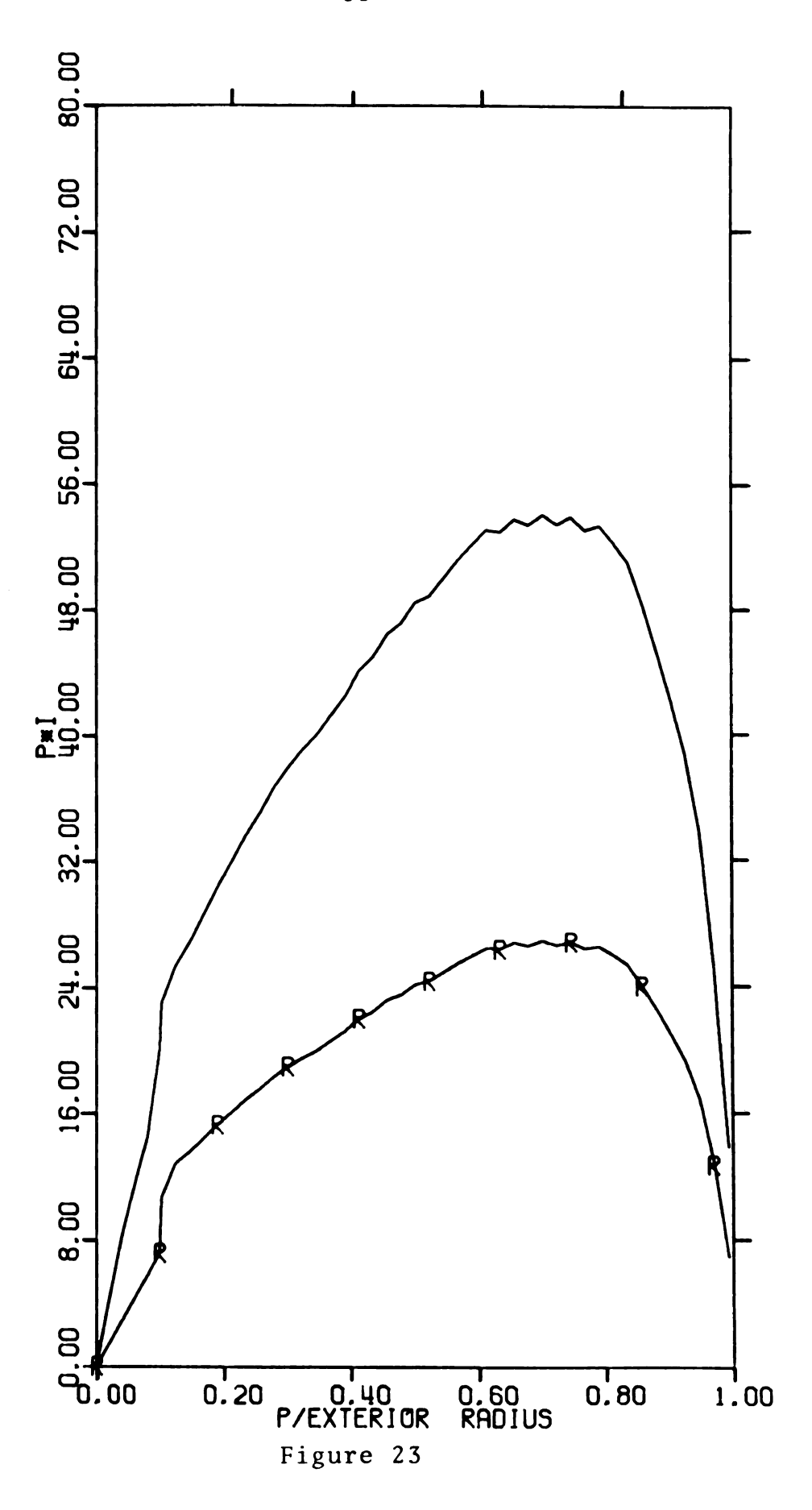
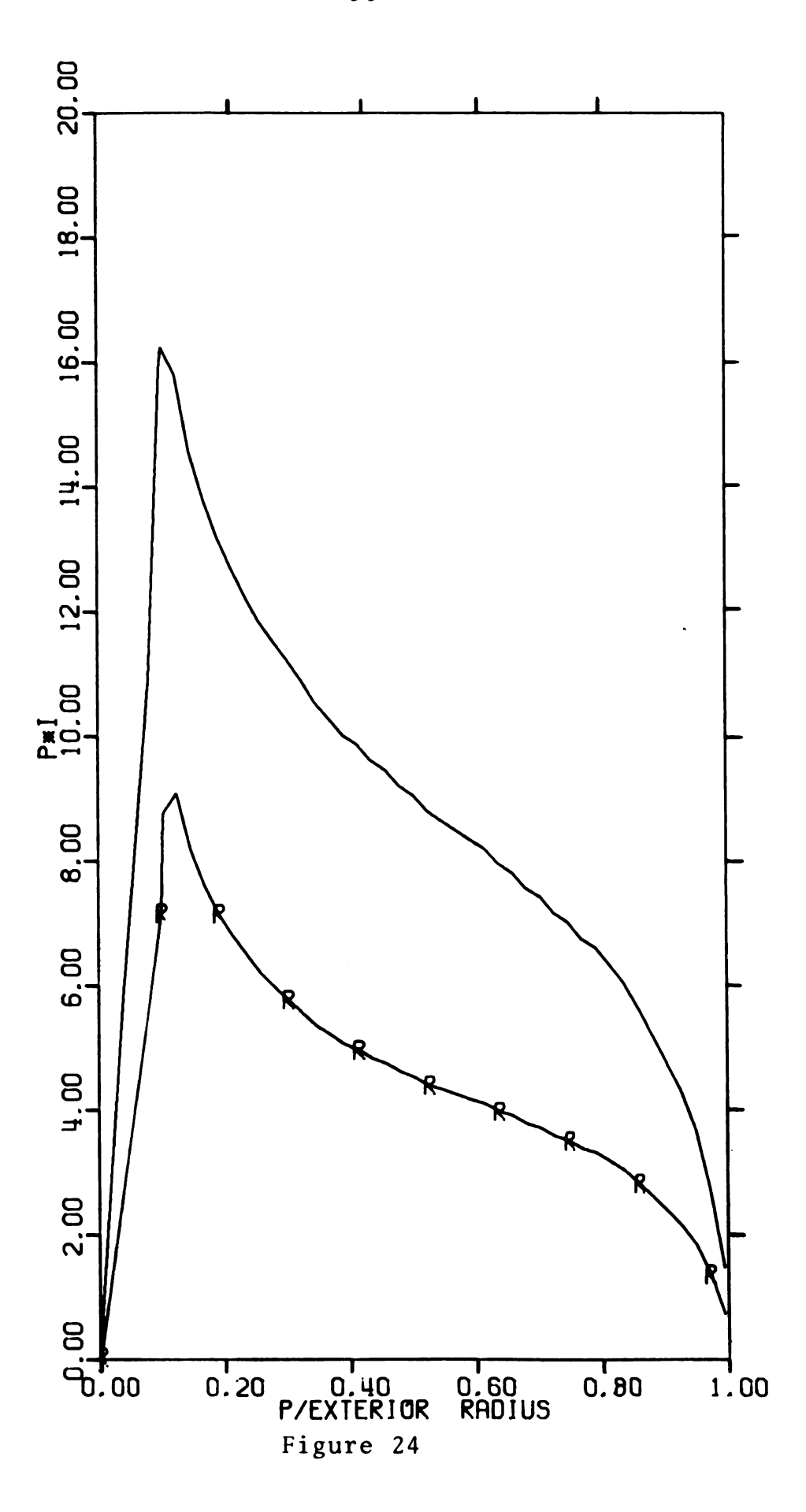


Figure 24. p I_{tot} and p I_r for a star with RR = 10, τ_o = 1000, ϵ = 0.001, B(r) = $5(r_c/r)I_c$, and ℓ = 0.5. Note that all the parameters but B coincide with the parameters in Figure 23.



which the results were moderately interesting; in a majority of the cases, even with the factor p adding weight to the curves at large impact parameter, most of the light was concentrated centrally (see Figures 21 and 22).

The curve p I_r for p < r_c is a straight line, under the assumption that I_c is constant. Observe that in the case of the infalling matter, we should change the interpretation of I_r , that now becomes the integral over the high frequency side of the line.

When $\epsilon\tau_0$ << 1, most of the light comes from the core, with only a small contribution from the p > r_c region. If $\epsilon\tau_0$ is increased to approximately 1, the contribution from the core becomes comparatively small, see Figure 23.

The appearance of the stars in the two wavelength bands chosen tend to parallel each other in a way that suggests there is little observational information to be obtained by interferometry in selected bands. On the other hand, we see that the image shown on Figure 23 is very different from the one on Figure 24, due to variation of excitation with radius, and both contrast strongly with Figures Thus some hope is offered of utility. While we 21 and 22. unfortunately did not construct similar plots for accelerating outflows, we may expect that in such cases, when the excitation in the atmosphere is small, one would observe a smaller image in emission near line center and larger ones far from line center. This is due to the concentration of low velocity material near the star core, and to

the large extension far from the star core of the high velocity material, in contrast with our decelerating flow case (see Figures 2 and 3).

CHAPTER IV

CONCLUSIONS AND FUTURE WORK

Conclusions

In summary, we come to the following conclusions:

- 1. The value of the source function is not very sensitive to the disconnected approximation, except at large radius. We found that the larger the value of $\varepsilon\tau_0$, the better the agreement between the approximate and the exact solution.
- 2. The whole analysis is rather sensitive to the outer cutoff radius. The line profile is the most sensitive part, and can develop an infinitely steep drop at the frequency corresponding to the first velocity surface on the near side contained entirely within the cutoff radius. This kind of behavior is hidden, evidently, for subordinate lines (Kuan and Kuhi 1975), and provides a crucial test of the decelerating models. The resonance profiles of N V, observed for several P Cygni stars by Hutchings (1976) do not exhibit the steep slope at the blue edge of emission that is present inall our calculated profiles. We conclude that insofar as this sample represents P Cygni stars, the model of Kuan and Kuhi does not seem to apply to such stars.

- 3. The extremely steep drop observed for large RR is highly suggestive of the C IV profile in the QSO PHL 5200, which Scargle, Caroff and Noerdlinger (1972) could not fit with any of their models. There is still a problem with the large equivalent width of C IV (when C III shows much symmetry), but an envelope somewhat elongated toward and away from the observer could handle that, by diverting C IV radiation to the side. The worst problem has always been the steep dropoff in C IV to the blue of line center. the present model, this would occur somewhat to the blue of true line center, but we have verified that for a reasonable RR, such as 100, the dropoff can come right at the edge of the QSO rest frequency within the tolerance of the observations. If this model can be further filled in, it could provide important evidence for the masses of QSOs, or the density of the intergalactic medium, whichever caused the deceleration.
- 4. The force is highly sensitive to any simplifying assumption, such as the disconnections.
- 5. The appearance of the star as could be observed interferometrically is not very exciting. Unless one adds a lot of emission from the envelope, it will be very faint, and the differences among different models are not likely to be decisive observationally.

A final point is that our models all apply equally

well to the case of accelerating infall. Hopefully, when better observations are available, we can compare profiles with observations of the stars discussed by Walker (1968, 1972). In the case of infall, we may expect more radical changes in ionization conditions at the place identified as \mathbf{r}_{m} , so the cutoff seems more plausible. Furthermore, in the case of infall, the mechanism (gravity) for acceleration seems readily comprehensible, while in the case of outflow, we have seen that for most reasonable combinations of parameters, gravity is insufficient to produce required deceleration, due to the much greater luminosity of these stars.

Future Work

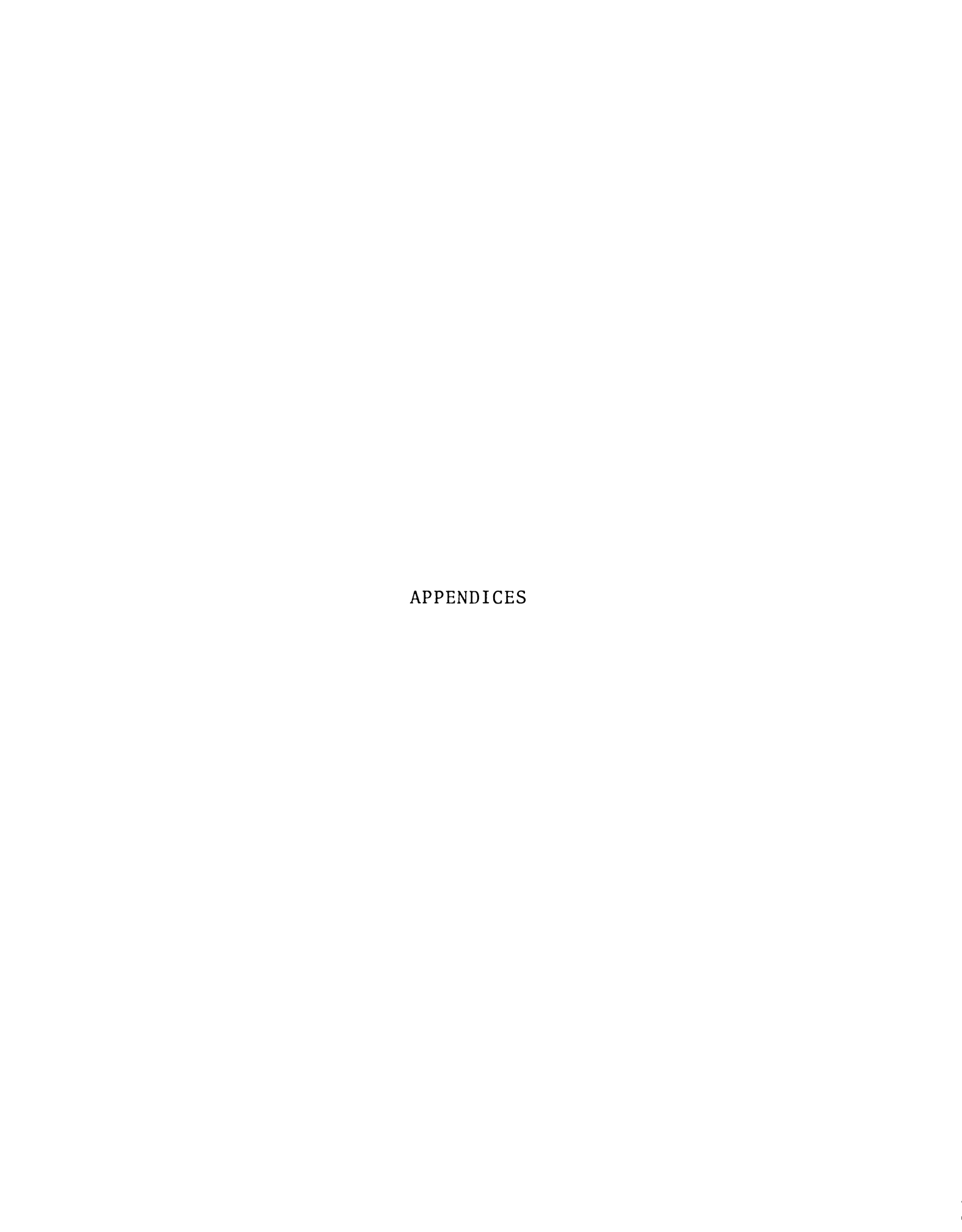
One of the drawbacks of our formulation is the assumption that the population of the lower level of the transition is much higher than the population of the upper one (see equation II-49). This is a good approximation for resonance lines or for lines like the C III λ 1175, where the lower level is a metastable one. These kinds of lines are usually in the ultraviolet region of the spectrum, which limits tremendously the observing possibilities. Our next step will then be to extend our formulation to the case of subordinate lines. We must find the populations of the upper and lower levels under conditions of Non Local Thermodynamic Equilibrium (NLTE).

We have to consider all the processes that tend to

populate or depopulate each level and solve simultaneously the rate equations and the transfer equation. Our equations will now be (II-27), (II-28), (II-29), and instead of the two-level atom excitation law (II-30), we will have a system of equations with the populations as unknowns.

Following Mihalas, Heasley, and Auer (1975) we consider an atmosphere composed of hydrogen and helium. The atomic model for hydrogen assumes 16 levels, allowing departures from equilibrium for the first five levels. For helium we assume a 16 level He I atom and a 32 level He II ion, with the possibility of having the first two levels of each ion under NLTE conditions.

The computation of the rate matrix involves the determination of the collisional excitation and de-excitation rates as well as the radiative transition rates for each pair of levels. Obviously, the fact that we must solve the equations for the whole atmosphere simultaneously, demands a very large storage capability.



APPENDIX A

Let da be an infinitesimal element of area, and P a point on it (in this Appendix we follow closely Cox and Giuli (1968) and Rybicki (1970)). The unit vector perpendicular to the surface is $\hat{\mathbf{n}}$, and $\hat{\mathbf{n}}$ is another vector that makes an angle θ with $\hat{\mathbf{n}}$. If $dE_{_{\mbox{$V$}}}$ is the energy that flows through da in time dt inside the solid angle $d\omega$ about the direction of $\hat{\mathbf{n}}$ with frequency between ν and ν + $d\nu$, we define the specific intensity $I_{_{\mbox{$V$}}}$ as

$$dE_{v} = I_{v} dv da \cos\theta d\omega dt$$
. (A-1)

 I_{ν} will be a function of frequency $\nu,$ position $\dot{\vec{r}},$ angle \hat{n} and time t.

When the beam of radiation passes through an element of mass dm, the energy in the beam with frequencies between ν and ν + d ν contained in the solid angle d ω will increase due to emission in the element of mass by the amount dE' $_{\nu}$ during the time dt, and it will be given by

$$dE'_{v} = j_{v} dv dm d\omega dt , \qquad (A-2)$$

 ${\rm j}_{_{\rm V}}$ being the mass emission coefficient. Note that it includes true emission as well as photon scattering into the beam from other directions. Similarly, we have an

absorption coefficient $\kappa_{_{\mbox{$V$}}}$ (true absorption and scattering out of the beam). If no emission occurs, the change in the specific intensity $I_{_{\mbox{$V$}}}$ of a beam traveling a distance ds through a medium of density ρ is given by

$$dI_{v} = -\kappa_{v} \rho I_{v} ds , \qquad (A-3)$$

where $\kappa_{_{\mbox{$V$}}}$ is the mass absorption coefficient. The corresponding change in energy is

$$dE''_{\nu} = -I_{\nu} \kappa_{\nu} \rho ds d\nu da \cos\theta d\omega dt . \qquad (A-4)$$

But ρ ds da $\cos\theta$ = dm, thus

$$dE'_{\nu} = j_{\nu} d\nu \rho ds da cos\theta d\omega dt$$
. (A-5)

The change in energy in the beam allowing for emission and absorption is then

$$dI_{\nu}d\nu da \cos\theta d\omega dt = (j_{\nu} - \kappa_{\nu}I_{\nu})\rho d\nu ds da \cos\theta d\omega dt$$
, (A-6)
or equivalently

$$\frac{dI}{\rho ds} = j_{v} - \kappa_{v} I_{v} , \qquad (A-7)$$

this being the general expression of the equation of transfer.

Let us consider now a frequency v_0 corresponding to the transition $j \to i$ in a given atom. The mass absorption coefficient κ_v will be a sharply peaked function with its maximum at the frequency corresponding to the line center

 v_0 . The line opacity in the rest frame of the material is

$$k_{y} = \rho \kappa_{y}$$
, (A-8)

and the integrated line opacity

$$k_{\ell}(\vec{r}) = \int_{0}^{\infty} k_{\nu}(\vec{r}) d\nu. \tag{A-9}$$

The normalized profile function is defined by

$$\phi(\vec{r}, \nu) = \frac{k_{\nu}(\vec{r})}{k_{\rho}(\vec{r})} . \qquad (A-10)$$

If the material that is absorbing and emitting is moving at high velocities with respect to the observer, we have to include the effect of the velocity field on the frequency. Different parts of the material will see the same photon at different frequencies. The normalized profile will now depend on the direction \hat{n} . Considering the Doppler effect to lowest order in v/c

$$\phi(\vec{r}, \hat{n}, \nu) = \phi(\vec{r}, \nu - \frac{\nu_0}{c} \hat{n} \cdot \vec{v}(\vec{r})) . \qquad (A-11)$$

Due to the sharpness of the absorption profile, this shift in frequency can produce a substantial change in the optical depth along the ray path in a moving atmosphere.

We can now write the transfer equation as

$$\hat{\mathbf{n}} \cdot \nabla \mathbf{I}_{\mathcal{V}}(\mathbf{r}, \hat{\mathbf{n}}) = \rho \, \mathbf{j}_{\mathcal{V}}(\mathbf{r}) - \mathbf{k}_{\mathcal{V}}(\mathbf{r}) \, \mathbf{I}_{\mathcal{V}}(\mathbf{r}, \hat{\mathbf{n}}) , \qquad (A-12)$$

$$\hat{\mathbf{n}} \cdot \nabla \mathbf{I}_{\mathcal{V}}(\vec{\mathbf{r}}, \hat{\mathbf{n}}) = \mathbf{k}_{\ell}(\vec{\mathbf{r}}) \phi(\vec{\mathbf{r}}, \mathbf{v} - \frac{\mathbf{v}_{0}}{c} \hat{\mathbf{n}} \cdot \vec{\mathbf{v}}(\vec{\mathbf{r}})) [S(\vec{\mathbf{r}}) - \mathbf{I}_{\mathcal{V}}(\vec{\mathbf{r}}, \hat{\mathbf{n}})], \quad (A-13)$$

where the source function S is defined as

$$S(r) = \frac{j_{\nu}(\vec{r})}{\kappa_{\nu}(r)} = \frac{N_{2}(\vec{r}) A_{21}}{N_{1}(\vec{r}) B_{12} - N_{2}(\vec{r}) B_{21}}, \quad (A-14)$$

where $N_2(\vec{r})$ and $N_1(\vec{r})$ are the number density of atoms in the upper and lower level respectively of the transition we are considering, and A_{21} , B_{21} , and B_{12} are the Einstein coefficients.

If T is a characteristic temperature in the atmosphere, we can define a typical Doppler velocity

$$\bar{v}_{th} = \left[\frac{2kT}{m}\right]^{\frac{1}{2}},$$
 (A-15)

and a Doppler shift

$$\Delta_{o} = \frac{v_{o} \overline{v}_{th}}{c} . \qquad (A-16)$$

Normalizing with this Doppler shift our frequency, referred to the line center, we obtain the dimensionless variable

$$x = \frac{v - v_0}{\Delta_0} , \qquad (A-17)$$

and the line profile

$$\phi(\vec{r},x) = \frac{1}{\sqrt{\pi} \delta(r)} \exp[-x^2/\delta^2(r)] , \qquad (A-18)$$

where

$$\delta(\mathbf{r}) = \frac{\mathbf{v}_{th}(\dot{\mathbf{r}})}{\dot{\mathbf{v}}_{th}} . \tag{A-19}$$

Using \overline{v}_{th} as the unit for velocities,

$$\vec{u}(\vec{r}) = \frac{\vec{v}(\vec{r})}{\vec{v}_{th}} , \qquad (A-20)$$

the equation of transfer becomes

$$\hat{\mathbf{n}} \cdot \nabla \mathbf{I}_{\mathbf{x}}(\vec{\mathbf{r}}, \hat{\mathbf{n}}) = \mathbf{k}_{\varrho} \phi(\vec{\mathbf{r}}, \mathbf{x} - \hat{\mathbf{n}} \cdot \vec{\mathbf{u}}(\vec{\mathbf{r}})) [S(\vec{\mathbf{r}}) - \mathbf{I}_{\mathbf{x}}] . \tag{A-21}$$

Notice that

$$x' = x - \hat{\mathbf{n}} \cdot \vec{\mathbf{u}}(\vec{\mathbf{r}}) = \left[v - v_0 - v_0 \frac{\hat{\mathbf{n}} \cdot \vec{\mathbf{v}}(\vec{\mathbf{r}})}{c} \right] \frac{1}{\Delta_0} , \qquad (A-22)$$

is the frequency seen by the material in the co-moving frame, measured from the line center in units of the thermal width. Using x' as independent variable instead of x, the mathematical identity for the gradient becomes

$$\hat{\mathbf{n}} \cdot \nabla \mathbf{I}_{\mathbf{X}}(\hat{\mathbf{r}}, \hat{\mathbf{n}}) = \hat{\mathbf{n}} \cdot \begin{bmatrix} \frac{3}{2} & \frac{1}{h_{\mathbf{j}}} & \frac{\partial \mathbf{I}_{\mathbf{X'}}}{\partial \mathbf{r}_{\mathbf{j}}} & \hat{\mathbf{e}}_{\mathbf{j}} - (\frac{1}{2} & \frac{\hat{\mathbf{n}}}{h_{\mathbf{j}}} & \frac{\partial \hat{\mathbf{u}}}{\partial \mathbf{r}_{\mathbf{j}}}) \frac{\partial \mathbf{I}_{\mathbf{X'}}}{\partial \mathbf{X'}} \end{bmatrix}$$

$$= \hat{\mathbf{n}} \cdot \nabla \mathbf{I}_{\mathbf{X'}} - Q(\hat{\mathbf{r}}, \hat{\mathbf{n}}) \frac{\partial \mathbf{I}_{\mathbf{X'}}}{\partial_{\mathbf{X'}}}, \qquad (A-23)$$

with

$$Q(\vec{r}, \hat{n}) = \sum_{j} \frac{n_{j}}{h_{j}} \hat{n} \cdot \frac{\partial \vec{u}}{\partial r_{j}} , \qquad (A-24)$$

and

$$h_{j} = \left[\left(\frac{\partial x}{\partial r_{j}} \right)^{2} + \left(\frac{\partial y}{\partial r_{j}} \right)^{2} + \left(\frac{\partial z}{\partial r_{j}} \right)^{2} \right]^{\frac{1}{2}} . \tag{A-25}$$

In spherical coordinates, and with $\vec{u} = u(r) \hat{e}_r$

$$\frac{\partial \vec{u}}{\partial \theta} = u \hat{e}_{\theta}$$
, $\frac{\partial \vec{u}}{\partial \phi} = u \sin \theta \hat{e}_{\phi}$, $\frac{\partial \vec{u}}{\partial r} = u \hat{e}_{r}$, (A-26)

$$Q(r,\hat{n}) = n_r^2 u' + n_\theta^2 \frac{u}{r} + n_\phi^2 \frac{u}{r} = \mu^2 u' + (1 - \mu^2) \frac{u}{r} , \quad (A-27)$$

being h_r = 1, h_θ = r, h_ϕ = r sin θ , and n_r = μ . The gradient, keeping x' constant is:

$$\hat{\mathbf{n}} \cdot \nabla \mathbf{I}_{\mathbf{X'}}(\mathbf{r}, \hat{\mathbf{n}}) = \mu \frac{\partial \mathbf{I}_{\mathbf{X'}}}{\partial \mathbf{r}} - \frac{(1 - \mu^2)^{\frac{1}{2}}}{\mathbf{r}} \frac{\partial \mathbf{I}_{\mathbf{X'}}}{\partial \theta}$$

$$= \mu \frac{\partial \mathbf{I}_{\mathbf{X'}}}{\partial \mathbf{r}} + \frac{(1 - \mu^2)}{\mathbf{r}} \frac{\partial \mathbf{I}_{\mathbf{X'}}}{\partial \theta} . \tag{A-28}$$

Collecting our results together

$$\hat{\mathbf{n}} \cdot \nabla \mathbf{I}_{\mathbf{X}}(\mathbf{r}, \hat{\mathbf{n}}) = \mu \frac{\partial \mathbf{I}_{\mathbf{X'}}}{\partial \mathbf{r}} + \frac{(1 - \mu^2)}{\mathbf{r}} \frac{\partial \mathbf{I}_{\mathbf{X'}}}{\partial \mu}$$

$$- \left[\mu^2 \mathbf{u'}(\mathbf{r}) + (1 - \mu^2) \frac{\mathbf{u}}{\mathbf{r}}\right] \frac{\partial \mathbf{I}_{\mathbf{X'}}}{\partial \mathbf{x'}} , \qquad (A-29)$$

and finally

$$\mu \frac{\partial I_{x'}}{\partial r} + \frac{(1-\mu^2)}{r} \frac{\partial I_{x'}}{\partial \mu} - [\mu^2 u'(r) + (1-\mu^2) \frac{u}{r}] \frac{\partial I_{x'}}{\partial x'} =$$

$$k_{g} \phi(r, \nu - \frac{\nu_{o}}{c} \hat{n} \cdot \vec{v}(r)) [S(r) - I_{\nu}(r, \hat{n})] . \qquad (A-30)$$

APPENDIX B

To solve equation (II-40) we approximated it by a system of linear equations in the n unknowns $S(r_1)$, $S(r_2)$, ..., $S(r_n)$, where

$$r_i = r_c + (i-1)(r_m - r_n)/(n-1)$$
 (B-1)

For each $r = r_i$ we obtain an integral equation that we discretize, substituting for each integral a sum, obtaining an equation of the form

$$\sum_{j=1}^{n} a_{ij} S(r_{j}) = H(r_{i}) I_{c} + \varepsilon B(r_{i})/(1 - \varepsilon) . \quad (B-2)$$

To obtain the weights a_{ij} we performed the integrals over z using trapezoidal rule, dividing the interval of integration in 250 steps. Given now the point (r,z) there is a constant v_z curve that passes through that point. Once this curve is determined we must find its other intersection with the p = constant line, where $p = (r^2 - z^2)^{\frac{1}{2}}$. This new intersection will be at r_2 , and r_2 is computed from equation (II-22) with $r_1 = -(r_2^2 - r_2^2)^{\frac{1}{2}}/r_2$. In obtaining r_2 we must solve a cubic equation in the $\ell = \frac{1}{2}$ case, and a quadratic equation in the $\ell = 1$ case.

The line of sight velocity is determined by

$$v_z = v_0 \frac{r_0^{\ell} z}{r^{\ell+1}} = v_0 \frac{r_0^{\ell} z_2}{r_2^{\ell+1}}$$
, (B-3)

and the impact parameter is

$$p = (r^2 - z^2)^{\frac{1}{2}} = (r_2^2 - z_2^2)^{\frac{1}{2}}.$$
 (B-4)

From these two equations we obtain

$$r^2 - z^2 = r_2^2 - (\frac{r_2}{r})^{2(\ell+1)} z^2$$
 (B-5)

In the $\ell = 1$ case, taking $u = (r_2/r)^2$, (B-5) reduces to

$$\left(\frac{z}{r}\right)^2 u^2 - u + 1 - \left(\frac{z}{r}\right)^2 = 0$$
, (B-6)

with solutions u = 1 and

$$u = \left(\frac{r}{z}\right)^2 - 1$$
 (B-7)

In the $\ell = \frac{1}{2}$ case, with $w = r_2/r$, equation (B-5) becomes

$$\left(\frac{z}{r}\right)^2 w^3 - w^2 + 1 - \left(\frac{z}{r}\right)^2 = 0$$
 (B-8)

As we know that w = 1 (known intersection) is a solution, we can reduce (B-8) to a quadratic equation. The positive root is

S

$$w = \frac{1}{2} \{ (\frac{r}{z})^2 - 1 + [(\frac{r}{z})^2 - 1]^{\frac{1}{2}} [(\frac{r}{z})^2 + 3]^{\frac{1}{2}} \}.$$
 (B-9)

Once r_2 was found, we determine the two "zones" that comprise this second intersection, i.e. $r_k \leq r_2 \leq r_{k+1}$. If we are solving the equation corresponding to $r = r_i$, we then have contributions to the terms a_{ik} , and a_{i-k+1} , that are determined by assigning linear weights depending on how close r_2 is to the zones r_k and r_{k+1} .

In the disconnected case, all terms in equation (II-40) containing a quantity subscripted 2 are discarded, then a_{ij} becomes diagonal, and the surviving terms are actually only integrals over μ = -z/r at fixed r; hence no interpolation procedure is needed. The trapezoidal rule with 100 steps was used.

We constructed the a_{ij} matrix a row at a time, and at the same time corresponding coefficients for equations (II-51) and (II-52) were computed and stored, later to be folded into the vector of S values, after it is found. A standard IMSL routine, LEQT2F, was used to solve the system of equations. Occasionally, fluctuations were encountered in S(r) and a(r) due to finite zoning, and these decreased slowly but steadily as the zoning was refined.

APPENDIX C

In the disconnected approximation, equation (II-43) yields

$$S(r)\left[\frac{\varepsilon}{1-\varepsilon} + \frac{1}{2r} \int_{-r}^{r} G(\tau) dz\right] = \frac{\varepsilon B}{1-\varepsilon} + \frac{I}{2r} \int_{-r}^{2e} G(\tau) dz , \qquad (C-1)$$

where $G(\tau)$ is defined in equation (II-38) and τ is evaluated at r, with direction cosine μ , given by μ = -z/r. If τ << 1, $G \simeq 1$ and the integrals are trivial, leading to

$$S(r)\left[\frac{\varepsilon}{1-\varepsilon} + 1\right] = \frac{\varepsilon}{1-\varepsilon} B + I_{c}\left(\frac{z_{e} + r}{2r}\right) , \qquad (C-2)$$

or simply

$$S(r) = \varepsilon B(r) + I_{c} W(r) (1 - \varepsilon) , \qquad (C-3)$$

where W(r) is the dilution factor given by (II-46). If $\tau >> 1$, $G(\tau) \simeq \tau^{-1} = \tau_r^{-1} \ell^{-1} |1-\mu^2(\ell+1)|$, (see equation II-22). In this case

$$\beta(r) = \frac{1}{2r} \int_{-r}^{r} G(\tau) dz \simeq \frac{1}{2\ell \tau_{r}} \int_{-1}^{1} |1 - \mu^{2}(\ell+1)| d\mu = \frac{1}{2\ell \tau_{r}} \left\{ \int_{-1}^{-(\ell+1)^{-\frac{1}{2}}} [\mu^{2}(\ell+1) - 1] d\mu + \int_{-(\ell+1)^{-\frac{1}{2}}}^{(\ell+1)^{-\frac{1}{2}}} [1 - \mu^{2}(\ell+1)] d\mu + \int_{-(\ell+1)^{-\frac{1}{2}}}^{1} [\mu^{2}(\ell+1) - 1] d\mu \right\}.$$

$$(C-4)$$

Carrying out the integration gives:

$$\beta(r) = \frac{1}{\ell \tau_r} \left[\frac{S^2}{3} \left(1 - \frac{2}{S^3} \right) - 1 + \frac{2}{S} \right] , \qquad (C-5)$$

where S = $(\ell+1)^{\frac{1}{2}}$. Defining $\mu_C = r_C/r$, the other integral is

$$\frac{1}{2\ell\tau_{\mathbf{r}}} \int_{-1}^{-(1-\mu_{\mathbf{c}}^{2})^{\frac{1}{2}}} |1-\mu^{2}(\ell+1)| d\mu . \qquad (C-6)$$

If $r/r_{c} > [(\ell+1)/\ell]^{\frac{1}{2}}$, the integral becomes

$$\frac{1}{2\ell\tau_{\mathbf{r}}} \int_{-1}^{-(1-\mu_{\mathbf{c}}^{2})^{\frac{1}{2}}} \left[\mu^{2}(\ell+1)-1\right] d\mu = \left\{\frac{\ell+1}{3} \left[1-(1-\mu_{\mathbf{c}}^{2})^{\frac{3}{2}}+(1-\mu_{\mathbf{c}}^{2})^{\frac{1}{2}}-1\right\} \times \frac{1}{2\ell\tau_{\mathbf{r}}} \right]. \tag{C-7}$$

For $\boldsymbol{\mu}_{\boldsymbol{C}}$ small, it is approximately

$$\frac{1}{4\tau_{r}} \mu_{c}^{2} = \frac{1}{4\tau_{r}} \left(\frac{r_{c}}{r}\right)^{2}. \tag{C-8}$$

Combining equations (C-1), (C-5), and (C-8), we obtain for

 $\tau >> 1$ and $r >> r_c$

$$S\left[\frac{\varepsilon}{1-\varepsilon} + \frac{1.177}{\tau_r}\right] \approx \frac{1}{4\tau_r} \frac{r_c^2}{r^2} + \frac{\varepsilon B}{1-\varepsilon} \quad \text{if } \ell = \frac{1}{2}$$
 (C-9)

and

$$S\left[\frac{\varepsilon}{1-\varepsilon} + \frac{0.6095}{\tau_r}\right] \simeq \frac{1}{4\tau_r} \frac{r_c^2}{r^2} + \frac{\varepsilon B}{1-\varepsilon}, \text{ if } \ell = 1. \tag{C-10}$$

We can obtain an approximate formula for the source function at the surface $(r = r_c)$, due to the fact that $z_e = 0$ and the integral in the right hand side of equation (C-1) is just $\beta(r)/2$. We have then for $r = r_c$

$$S_c\left[\frac{\varepsilon}{1-\varepsilon} + \frac{1.177}{\tau_r}\right] \simeq \frac{1.177}{2\tau_r} + \frac{\varepsilon B}{1-\varepsilon}$$
, if $\ell = \frac{1}{2}$, (C-11)

and

$$S_{c}\left[\frac{\varepsilon}{1-\varepsilon} + \frac{0.6095}{\tau_{r}}\right] \simeq \frac{0.6095}{2\tau_{r}} + \frac{\varepsilon B}{1-\varepsilon}, \text{ if } \ell = 1. \tag{C-12}$$



LIST OF REFERENCES

Allen, C.W. 1973, Astrophysical Quantities (3rd ed.; London: Athlone Press).

Beals, C.S. 1929, M.N.R.A.S., 90, 202.

----. 1930, Pub. Dom. Ap. Obs., 4, 271.

——. 1934, Pub. Dom. Ap. Obs., 6, 95.

Castor, J.I. 1970, M.N.R.A.S., 149, 111.

Castor, J.I., and van Blerkom D. 1970, Ap. J., 161, 485.

Castor, J.I., and Nussbaumer, H. 1972, M.N.R.A.S., 155, 293.

Chandrasekhar, S. 1934, M.N.R.A.S., 94, 522.

——. 1945, Rev. Mod. Phys., 17, 138.

Conti, P.S. 1972, Ap. J. Letters, 174, L79.

Cox, J.P., and Giuli, R.T. 1968, <u>Principles of Stellar Structure</u>, (New York: Gordon and Breach).

DeGroot, M. 1973, in Wolf-Rayet and High Temperature Stars, ed. M. K. V. Bappu and J. Sahade (Dordrecht: Reidel).

Gerasimovic, B. 1933, <u>Zs. f. Ap.</u>, <u>7</u>, 335.

Hummer, D.G. 1976, in <u>IAU Symposium No. 70</u>, ed. A. Sletteback (Dordrecht: Reidel).

Hutchings, J.B. 1976, Ap. J., 204, L99.

Kuan, P. 1975, Ap. J., 202, 425.

Kuan P., and Kuhi, L.V. 1975, Ap. J., 199, 148.

Kuhi, L.V. 1964, Ap. J., 140, 1409.

Lamers, H.J.G.L.M., and Morton, D.C. 1976, Ap. J. Suppl., 32, 715.

McCrea, W.H., and Mitra, K.K. 1936, Zs. f. Ap., 11, 359.

- Mihalas, D. 1970, <u>Stellar Atmospheres</u> (San Francisco: Freeman).
- Mihalas, D., Heasley, J.N., and Auer, L.H. 1975, NCAR-TN/STR-104, A Non-LTE Model Stellar Atmosphere Computer Program.
- Mihalas, D., Kunasz, P.B., and Hummer, D.G. 1975, Ap. J., 202, 465.
- ——. 1976a, Ap. J., 203, 647.
- ----. 1976b, Ap. J., 206, 515.
- Milne, E.A. 1926, M.N.R.A.S., 86, 459.
- Noerdlinger, P.D., and Rybicki, G.B. 1974, Ap. J., 193, 651.
- Oegerle, W.R., and van Blerkom, D. 1976A, Ap. J., 206, 150.
- ____. 1976b, Ap. J., 208, 453.
- Rublev, S.V. 1961, Soviet Astr. A. J., 4, 780.
- ——. 1963, <u>Soviet Astr. A. J.</u>, <u>6</u>, 686.
- ——. 1964, Soviet Astr. A. J., 7, 492.
- Rybicki, G.B. 1970, in <u>Spectrum Formation in Stars With</u> <u>Steady-State Extended Atmospheres</u>. eds. H. Groth and P. Wellman, (Washington: Gov. Printing Office).
- Scargle, J.D., Caroff, L.J., and Noerdlinger, P.D. 1970, Ap. J., 161, L115.
- Snow, T.P., and Marlborough, J.M. 1976, Ap. J., 203, L87.
- Sobolev, V.V. 1958, in <u>Theoretical Astrophysics</u>, ed. V.A. Ambartsumian (New York: Pergamon Press).
- Harvard Univ. Press). (Cambridge:
- Walker, M.L. 1968, in <u>Non-periodic Phenomena in Variable Stars</u>, ed. L. Detre (Budapest: Academic Press).
- ——. 1972, Ap. J., 175, 89.

